

# 1 **Cosmogenic ages indicate no MIS 2 refugia in the Alexander** 2 **Archipelago, Alaska**

3

4 Caleb K. Walcott<sup>1</sup>, Jason P. Briner<sup>1</sup>, James F. Baichtal<sup>2</sup>, Alia J. Lesnek<sup>3</sup>, Joseph M. Licciardi<sup>4</sup>5 <sup>1</sup>Department of Geology, University at Buffalo, Buffalo, NY 14260, USA6 <sup>2</sup>Tongass National Forest, Thorne Bay, AK 99919, USA7 <sup>3</sup>School of Earth and Environmental Sciences, CUNY Queens College, Flushing, NY 11367,  
8 USA9 <sup>4</sup>Department of Earth Sciences, University of New Hampshire, Durham, NH 03824, USA10 *Correspondence to:* Caleb K. Walcott ([ckwalcot@buffalo.edu](mailto:ckwalcot@buffalo.edu))

11

## 12 **Abstract**

13

14 The late-Pleistocene history of the coastal Cordilleran Ice Sheet remains relatively  
15 unstudied compared to chronologies of the Laurentide Ice Sheet. Yet accurate reconstructions of  
16 Cordilleran Ice Sheet extent and the timing of ice retreat along the Pacific Coast are essential for  
17 paleoclimate modeling, assessing meltwater contribution to the North Pacific, and determining  
18 the availability of ice-free land along the coastal Cordilleran Ice Sheet margin for human  
19 migration from Beringia into the rest of the Americas. To improve the chronology of Cordilleran  
20 Ice Sheet history in the Alexander Archipelago, Alaska, we applied <sup>10</sup>Be and <sup>36</sup>Cl dating to  
21 boulders and glacially sculpted bedrock in areas previously hypothesized to have remained ice-  
22 free throughout the local Last Glacial Maximum (LLGM; 20-17 ka). Results indicate that these  
23 sites, and more generally the coastal northern Alexander Archipelago, became ice-free by 15.1 ±  
24 0.9 ka (n = 12 boulders; 1 SD). We also provide further age constraints on deglaciation along the  
25 southern Alexander Archipelago and combine our new ages with data from two previous studies.  
26 We determine that ice retreated from the outer coast of the southern Alexander Archipelago at

27  $16.3 \pm 0.8$  ka ( $n = 14$  boulders; 1 SD). These results collectively indicate that areas above  
28 modern sea level that were previously mapped as glacial refugia were covered by ice during the  
29 LLGM until between  $\sim 16.3$  and  $15.1$  ka. As no evidence was found for ice-free land during the  
30 LLGM, our results suggest that previous ice-sheet reconstructions underestimate the regional  
31 maximum Cordilleran Ice Sheet extent, and that all ice likely terminated on the continental shelf.  
32 Future work should investigate whether presently submerged areas of the continental shelf were  
33 ice-free.

34

## 35 **1 Introduction**

36 The late-Pleistocene history of the coastal Cordilleran Ice Sheet remains relatively  
37 unstudied compared to chronologies of the Laurentide Ice Sheet (Dalton et al., 2020).  
38 Cordilleran Ice Sheet margin reconstructions from the Pacific Coast are based largely on  
39 qualitative field observations with little chronologic control (Dyke, 2004; Carrara et al., 2007;  
40 Dalton et al., 2020). While a few studies have recently generated local ice sheet retreat  
41 chronologies from terrestrial locations along the Pacific Coast (Darvill et al., 2018; Lesnek et al.,  
42 2018; Lesnek et al., 2020), there are still large areas of the southeastern Alaskan coastline that  
43 lack direct age constraints on deglaciation (Fig. 1). Much of the Northern Hemisphere was  
44 covered by continental ice sheets during the global Last Glacial Maximum (GLGM;  $\sim 26 - 19$   
45 ka). Chronologies of northern hemisphere glaciation have revealed that while the Laurentide Ice  
46 Sheet and many alpine glaciers worldwide were at their greatest extents during the global Last  
47 Glacial Maximum (GLGM;  $\sim 26-19$  ka), the coastal Cordilleran Ice Sheet and the Puget Lobe  
48 reached their maximum size  $\sim 20 - 17$  cal ka (local Last Glacial Maximum; hereafter LLGM ;  
49 Porter and Swanson, 1998; Booth et al., 2003; Praetorius and Mix, 2014; Darvill et al., 2018;

50 Lesnek et al., 2018). Other studies have also explored the Cordilleran Ice Sheet contributions to  
51 meltwater pulse 1A (~14.6 ka) following the saddle collapse between the Laurentide Ice Sheet  
52 and Cordilleran Ice Sheet (Gregoire et al., 2016; Ivanovic et al., 2017). Improved constraints on  
53 Cordilleran Ice Sheet history around the time of meltwater pulse 1A are necessary to elucidate  
54 any influences of coastal Cordilleran Ice Sheet configuration and retreat on saddle collapse.  
55 Additionally, numerical modeling studies show differing responses of the Cordilleran Ice Sheet  
56 to last deglacial climate oscillations, thus highlighting the need for an improved Cordilleran Ice  
57 Sheet chronology to bolster model improvement and validation (Tarasov et al., 2012; Seguinot et  
58 al., 2014; Gregoire et al., 2016; Seguinot et al., 2016; Ivanovic et al., 2017). Finally, a temporally  
59 accurate paleogeographic reconstruction of the coastal Cordilleran Ice Sheet margin is required  
60 to assess whether a viable coastal route existed for early Americans migrating from Beringia into  
61 the Americas. This route hinges on the presence of ice-free land (refugia) suitable for human  
62 habitation during the migration event(s). Earlier mapping efforts and other supporting  
63 information indicate areas of potential refugia along the former coastal Cordilleran Ice Sheet  
64 margin (Demboski et al., 1999; Cook et al., 2001; Carrara et al., 2003; Carrara et al., 2007;  
65 Shafer et al., 2010; Shafer et al., 2011; Hebda et al., 2022).

66 This study has two goals: 1) improve the spatio-temporal patterns of coastal Cordilleran  
67 Ice Sheet deglaciation in southeastern Alaska, and 2) assess whether areas of the northern  
68 Alexander Archipelago mapped as refugia were ice-free throughout the LLGM and thus  
69 available for human habitation (Fig. 2). We report 25 new cosmogenic  $^{10}\text{Be}$  exposure ages from  
70 boulders and bedrock in the northern Alexander Archipelago – the first exposure ages  
71 documenting Cordilleran Ice Sheet retreat from this coastal region. We also report four  $^{10}\text{Be}$  and  
72 four cosmogenic  $^{36}\text{Cl}$  ages from Suemez Island in the southern Alexander Archipelago. Our data

73 constrain the deglaciation of the marine-terminating Cordilleran Ice Sheet margin and expand the  
74 overall North Pacific coastal glacial chronology. Our results suggest deglaciation of coastal  
75 regions ~15.4 – 14.8 ka in the northern Alexander Archipelago and do not support previous  
76 mapping of refugia in areas that are presently above sea level.

77

## 78 **2 Setting**

79

80 The Alexander Archipelago, southeast Alaska, stretches ~480 km (Fig. 2) along the  
81 western coast of British Columbia. The southern part of the archipelago is dominated by Prince  
82 of Wales Island and surrounding islands, whereas the northern part encompasses Baranof and  
83 Chichagof Islands and a collection of smaller islands. The Alexander Archipelago consists of  
84 accreted terranes (Triassic to Cretaceous in age) with quartz-bearing diorite and granodiorite  
85 units and notable Eocene-Miocene granitic intrusive complexes (Wilson et al., 2015). Late-  
86 Pleistocene volcanic activity on southern Kruzof Island formed the Mt. Edgecumbe volcanic  
87 field (Riehle, 1996). Post-LLGM (late-Pleistocene and Holocene) eruptions formed extensive  
88 andesite flows on the island and blanketed much of the surrounding area with tephra (Riehle et  
89 al., 1984; Riehle et al., 1992; Riehle, 1996). Modern climate of the Alexander Archipelago is  
90 dominated by cool, wet summers and mild winters, with perennial heavy rainfall - Sitka (Baranof  
91 Island) receives ~2200 mm/yr while Chichagof Island receives over 3300 mm/yr (Ager, 2019;  
92 <https://wrcc.dri.edu/summary/Climsmak.html>). Snowfall is minimal at lower elevations, but  
93 more substantial in higher elevation areas (<https://wrcc.dri.edu/summary/Climsmak.html>).  
94 Glaciers occupy alpine cirques in the Alexander Archipelago (totaling < 150 km<sup>2</sup>), primarily on  
95 Baranof and Chichagof islands (Molnia, 2008). Presently, low-elevation (< 700 m asl) areas of

96 the archipelago are dominated by coniferous rainforests, while alpine tundra exists above the tree  
97 line (> 700 m asl; Ager, 2019).

98         Previous mapping shows much, if not all, of southeast Alaska covered by the Cordilleran  
99 Ice Sheet during the LLGM and the last deglaciation, with a maximum position likely  
100 terminating several kilometers out on the continental shelf of the Gulf of Alaska (Carrara et al.,  
101 2007). Ice caps formed atop the Coast Mountains and high massifs of the Alexander Archipelago  
102 coalesced and flowed westward to the continental shelf and the Pacific Ocean (Capps, 1932;  
103 Mann, 1986; Mann and Hamilton, 1995). Outlet glaciers occupied the present fjord and strait  
104 landscape (Carrara et al., 2007). Today, the landscape is strewn with clear indicators of  
105 widespread glaciation including deep fjords, glacially sculpted bedrock draped with boulders,  
106 and a variety of other glacial landforms, but it remains unclear whether all of southeast Alaska  
107 was covered by the Cordilleran Ice Sheet during the LLGM. Some areas of the Alexander  
108 Archipelago, presently above sea level, are hypothesized to have been ice-free throughout the  
109 LLGM (Carrara et al., 2007). Recent studies using <sup>10</sup>Be surface exposure dating of glacial  
110 landforms, however, indicate that some of these purported ice-age refugia in the southern  
111 Alexander Archipelago were covered by the Cordilleran Ice Sheet during its LLGM advance  
112 (Lesnek et al., 2018). Other areas previously mapped as ice age refugia in the northern Alexander  
113 Archipelago (Carrara et al., 2007; Dalton et al., 2020) are investigated in this study; if their  
114 presence is confirmed with numerical dating techniques, this would be a significant confirmation  
115 of the existence of coastal refugia.

116

117

## 118 **3 Methods**

119

### 120 **3.1 Boulder and bedrock sampling**

121

122           We collected 29 samples (11 bedrock, 18 boulder) for cosmogenic  $^{10}\text{Be}$  surface exposure  
123 dating (hereafter  $^{10}\text{Be}$  dating) during summer 2018, 2019, and 2020 (Figs. 3 and 4) from several  
124 sites in coastal Southeast Alaska, including Suemez ( $n = 4$ ), Baranof ( $n = 11$ ), Biorka ( $n = 4$ ),  
125 Kruzof ( $n = 4$ ) and Chichagof ( $n = 6$ ) islands. Our samples range in elevation from  $\sim 50$  to  $\sim 930$   
126 m asl; all sites are above the local marine limits of  $\sim 10 - 20$  m asl (Baichtal et al., 2021). We  
127 preferentially sampled paired sites consisting of stable boulders and neighboring unvegetated  
128 bedrock surfaces. This strategy allowed us to assess whether bedrock surfaces contain isotopic  
129 inheritance and provides insights into ice-sheet erosion history. In the absence of suitable  
130 boulders at a few locations, we sampled bedrock with clear evidence of glacial erosion to  
131 mitigate the possibility of  $^{10}\text{Be}$  inheritance.

132           We also collected samples from four glacially-transported boulders on the southwestern  
133 portion of Suemez Island for  $^{36}\text{Cl}$  surface exposure dating during the summer 2019 field season  
134 (Figs. 5; 6; Table 2). The boulders consist of non-vesicular olivine basalt of “Tertiary to  
135 Quaternary” age (Eberlein et al., 1983).

136           Surface samples were collected from the upper few centimeters of the boulders and  
137 bedrock using a handheld angle grinder, hammer, and chisel. We avoided sampling areas of the  
138 boulder tops and bedrock surfaces with visible signs of surface erosion (e.g., fractures,  
139 weathering pits). We did, however, observe erosional features on the boulders sampled for  $^{36}\text{Cl}$   
140 dating. We avoided collecting material from these areas, instead sampling parts of the basaltic  
141 boulder tops that showed fresh, unweathered surfaces. We recorded sample locations with a

142 handheld GPS unit or GAIA GPS (both with a vertical uncertainty of  $\pm 5$  m) and measured  
143 topographic shielding in the field with a clinometer and compass.

144

### 145 **3.2 $^{10}\text{Be}$ dating**

146

147 We processed samples at the University at Buffalo Cosmogenic Isotope Laboratory  
148 following established quartz purification and beryllium extraction procedures (e.g., Corbett et al.,  
149 2016). After quartz purification, we dissolved samples in hydrofluoric acid with precisely  
150 weighed  $^9\text{Be}$  carrier (PRIME Lab 2017.11.17-Be #3/#4;  $^9\text{Be}$  concentration of  $1074 \pm 8$  ppm). We  
151 isolated, oxidized, and packed beryllium into target cathodes in five different batches for  
152 accelerator mass spectrometer (AMS) analysis at PRIME lab at Purdue University. The samples  
153 were measured with respect to the 07KNSTD standard ( $^{10}\text{Be}/^9\text{Be}$  ratio of  $2.85 \times 10^{-12}$ ; Nishiizumi  
154 et al., 2007). We corrected sample ratios using batch-specific blank values between  $7.50 \times 10^{-16}$   
155 and  $3.14 \times 10^{-15}$ . AMS analytical uncertainty ranged from 3.2 to 7.3% with an average value of  
156 4.7%.

157 We calculated all  $^{10}\text{Be}$  ages using version 3 of the CRONUS-Earth exposure age  
158 calculator (hess.ess.washington.edu; Balco et al., 2008; Balco, 2017), using the Arctic production  
159 rate (Young et al., 2013) and a time-dependent ( $L_m$ ) scaling scheme (Lal, 1991).

160

### 161 **3.3 $^{36}\text{Cl}$ dating**

162

163 All whole rock samples were prepared at the University of New Hampshire Cosmogenic  
164 Isotope Laboratory using a modified version of the protocols in Stone et al. (2000) and Licciardi  
165 et al. (2008). After samples were crushed, etched in nitric acid, and homogenized, total sample  
166 chloride was measured on a  $\sim 1$  g aliquot of rock that was spiked with a small amount of  $^{37}\text{Cl}$ -

167 enriched solution (LLNL Spike A;  $^{35}\text{Cl}/^{37}\text{Cl} = 0.93$ ;  $1285 \pm 3$  ppm Cl) and a carrier containing  
168  $\sim 4000$   $\mu\text{g}$  of Br. Cl was extracted as  $\text{Ag}(\text{Cl},\text{Br})$  following standard procedures and chlorine  
169 concentrations were determined through isotope dilution of  $^{35}\text{Cl}/^{37}\text{Cl}$  ratios (Faure, 1986).  $^{36}\text{Cl}$   
170 was extracted from full rock samples as  $\text{Ag}(\text{Cl},\text{Br})$  after adding a carrier containing  $\sim 4800$   $\mu\text{g}$  of  
171 Br and a natural ratio Cl carrier ( $^{35}\text{Cl}/^{37}\text{Cl} = 3.127$ ;  $1436 \pm 9$  ppm Cl) to increase the size of the  
172 final precipitate.

173  $^{35}\text{Cl}/^{37}\text{Cl}$  and  $^{36}\text{Cl}/\text{Cl}$  ratios were measured at the Center for Accelerator Mass  
174 Spectrometry at Lawrence Livermore National Laboratory. Analytical uncertainty on  $^{35}\text{Cl}/^{37}\text{Cl}$   
175 measurements ranged from 0.04% to 0.43%; analytical uncertainty on  $^{36}\text{Cl}/\text{Cl}$  measurements  
176 ranged from 2.12% to 2.87%. Major and trace element analyses were conducted by SGS  
177 Minerals Services in Burnaby, British Columbia, Canada. Reported total Cl and  $^{36}\text{Cl}$   
178 concentrations are corrected for batch-specific process blanks (Table 2). Analytical data used to  
179 determine surface exposure ages are provided in supplementary tables S1 and S2.  $^{36}\text{Cl}$  exposure  
180 ages were calculated using an in-development version of the CRONUS-Earth  $^{36}\text{Cl}$  calculator  
181 ([http://stoneage.ice-d.org/math/Cl36/v3/v3\\_Cl36\\_age\\_in.html](http://stoneage.ice-d.org/math/Cl36/v3/v3_Cl36_age_in.html)) and Lm scaling (Lal, 1991).

182

### 183 **3.4 Exposure age calculation considerations**

184

185 We made no corrections for post-glacial elevation changes or snow cover when  
186 calculating our  $^{10}\text{Be}$  and  $^{36}\text{Cl}$  ages. Post-glacial isostatic adjustment results in a time-varying rate  
187 of cosmogenic nuclide production (Jones et al., 2019). This effect can be corrected for using  
188 comprehensive records of regional emergence constrained by glacial isostatic adjustment models  
189 or relative sea-level histories. Hundreds of radiocarbon ages constrain the relative sea level  
190 chronology in the Alexander Archipelago; the sites in our study experienced  $\sim 50$  m of relative



191 sea level lowering due to forebulge collapse between ~15 and 10 ka (Baichtal et al., 2021).  
192 Corrections for glacial isostatic adjustment history, albeit slightly uncertain given site-to-site  
193 differences in elevation history, result in small changes (~1% age decrease), and thus we report  
194 our ages without any correction for isostatic adjustment (Tables 1 and 2). Furthermore, changes  
195 in air pressure near a retreating ice margin and shifts in air compression above a sample site that  
196 experienced elevation change may mitigate any effects of isostatic adjustment on cosmogenic  
197 nuclide production, potentially rendering any elevation correction unnecessary (Staiger et al.,  
198 2007).

199         Extended periods of thick and dense snow cover can also inhibit  $^{10}\text{Be}$  and  $^{36}\text{Cl}$  production  
200 in a rock surface and lead to erroneously young apparent exposure ages. While modern snowfall  
201 reports for lower-elevation areas of the Alexander Archipelago indicate minimal average  
202 wintertime snow cover (10 – 20 cm; <https://wrcc.dri.edu/summary/Climsmak.html>), there are no  
203 data for higher-elevation areas. Consequently, we cannot report our ages with reliable snow  
204 shielding corrections and these exposure dates should be considered minimum ages. However,  
205 most of our sites are from low to moderate elevations (<500 m asl; Table 1).

206         Post-depositional weathering and erosion can also affect exposure ages. We observed  
207 fresh, unweathered glacially scoured bedrock across all our field sites, indicating minimal post-  
208 glacial erosion. We made no corrections for erosion in our age calculations presented within the  
209 manuscript text and thus these should be considered minimum ages. For sensitivity purposes, we  
210 calculated ages using an erosion rate of 0.3 cm/kyr, similar to erosion rates applied nearby in  
211 British Columbia (Menounos et al., 2017). These erosion-corrected ages are between 2% and 7%  
212 older and are found in Tables S3 and S4.

213 Both cosmogenic and nucleogenic  $^{36}\text{Cl}$  can be present in rock surfaces, and for our  
214 surface exposure age calculations we assumed steady state production/decay of nucleogenic  $^{36}\text{Cl}$ .  
215 Moderate amounts of nucleogenic  $^{36}\text{Cl}$  are produced when  $^{35}\text{Cl}$  absorbs neutrons released by the  
216 decay of U and Th isotopes (Gosse and Phillips, 2001). However, because the formation age of  
217 the sampled basalt flow on Suemez Island is loosely constrained to the “Tertiary to Quaternary”  
218 (Eberlein et al., 1983), nucleogenic  $^{36}\text{Cl}$  production/decay may or may not be in steady state. To  
219 assess the sensitivity of our exposure ages to the assumption of steady state nucleogenic  $^{36}\text{Cl}$   
220 production, we also calculated exposure ages using a rock formation age of 20 ka, which, given  
221 the timing of the LLGM ice advance in Southeast Alaska (Lesnek et al., 2018), is the youngest  
222 formation age we might expect for these rocks. Results of this test (Table S3) show that  
223 calculated  $^{36}\text{Cl}$  ages are relatively insensitive to rock formation age (<1% surface exposure age  
224 increase in all cases), which is well within total uncertainty.

225

## 226 **4 Results**

227

228 We sampled from the summit of a massif at ~410 m asl on south-central Suemez Island  
229 (southern Alexander Archipelago) and from a flat bench scattered with boulders on the summit’s  
230 flank for  $^{10}\text{Be}$  dating (Fig. 6). The two boulders sampled on the bench date to  $15.6 \pm 0.7$   
231 (19SEAK-07; Fig. 3) and  $15.0 \pm 1.1$  ka (19SEAK-08; we report all surface exposure ages with 1  
232  $\sigma$  internal uncertainty; Table 1). The summit site featured fresh glacially sculpted bedrock  
233 surfaces with a couple boulders resting on the bedrock. A boulder and its adjacent bedrock  
234 surface, as a pair, date to  $17.4 \pm 1.2$  (19SEAK-09) and  $19.7 \pm 1.2$  ka (19SEAK-10), respectively  
235 (Fig. 3). The three boulders yield a mean age of  $16.0 \pm 1.2$  ka ( $n = 3$ ; 1 SD).

236 On southwestern Suemez Island, we sampled four large boulders for  $^{36}\text{Cl}$  dating. The  
237 boulders were distributed across a terrain of patchy muskeg with locally outcropping bedrock.  
238 Based on reconstructed Cordilleran Ice Sheet flow directions (Lesnek et al., 2020) and boulder  
239 composition (supplementary table S2; Eberlein et al., 1983), the boulders were likely plucked  
240 from basalt flows present on the southwestern portion of Suemez Island (Brew, 1996). The four  
241 basalt boulders from southwestern Suemez Island have  $^{36}\text{Cl}$  exposure ages ranging from  $12.4 \pm$   
242  $0.3$  to  $16.4 \pm 0.5$  ka (ages are reported at  $1 \sigma$  internal uncertainty; Fig. 5; Table 2).  $^{36}\text{Cl}$  surface  
243 exposure ages assuming 3 mm/ka of surface erosion and non-steady state nucleogenic  $^{36}\text{Cl}$   
244 production are presented in Table S3; for all four samples, changing these parameters results in  
245 calculated surface exposure ages  $<2\%$  higher than those presented in the main text.

246 We collected samples from four sites (Baranof Sites A – D; Fig. 7) on the ocean-facing  
247 side of Baranof Island, northern Alexander Archipelago. Here, we chose our helicopter ground  
248 stops in an area previously mapped as ice-free throughout the LLGM (Carrara et al., 2007; Fig.  
249 7). Evidence for glacial sculpting of bedrock surfaces is clear; glacial grooves, striations and  
250 chatter marks are present at all sites, and the bedrock surfaces, in places, are topped by perched  
251 boulders (Fig. 3). Field evidence of recent glaciation, including relatively unweathered chatter  
252 marks, grooves, and striations, contradicts prior mapping of these areas being ice-free during the  
253 LLGM.

254 Baranof Site A is a large, unforested area of bedrock outcrops composed of several  
255 smaller ridges. Here, we sampled two bedrock surfaces – one from the stoss side of a bedrock  
256 outcrop (19SEAK-18; Fig. 3) and one from the top surface of a nearby bedrock patch (19SEAK-  
257 19) – which date to  $21.7 \pm 0.9$  and  $28.0 \pm 1.1$  ka, respectively. A boulder sampled adjacent to  
258 bedrock (sample 19SEAK-18) yielded an exposure age of  $16.9 \pm 0.8$  ka (19SEAK-17). A second

259 boulder sample from this site dates to  $14.4 \pm 0.7$  ka (19SEAK-20; Fig. 3). At Baranof Site B – a  
260 raised bedrock knob – we sampled two boulders and one bedrock surface. The two boulders have  
261  $^{10}\text{Be}$  ages of  $15.1 \pm 0.6$  ka (19SEAK-23; Fig. 3),  $14.4 \pm 0.7$  ka (19SEAK-21); the bedrock sample  
262 has a  $^{10}\text{Be}$  age of  $14.4 \pm 0.6$  ka (19SEAK-22). Baranof Site C is a high ridge between the ocean  
263 and a U-shaped valley with abundant bedrock outcrops and few boulders. Here, a boulder yielded  
264 an exposure age of  $16.3 \pm 0.6$  ka (19SEAK-24; Fig. 3) whereas a bedrock surface dates to  $15.7 \pm$   
265  $0.6$  ka (19SEAK-25). Finally, Baranof Site D is a small bedrock ridge between two peaks with  
266 massive stoss and lee features. At this site, we collected samples from two quartz veins in the  
267 bedrock, which have exposure ages of  $18.2 \pm 0.7$  (19SEAK-26; Fig. 3) and  $20.2 \pm 0.8$  ka  
268 (19SEAK-27). Because the sites are all in relatively close proximity and from similar elevations  
269 (50 – 160 m asl), we treat the samples as having experienced the same glacial history, and thus  
270 should belong to a single age population. Collectively, boulder samples yield a mean age of  $15.4$   
271  $\pm 1.1$  ka ( $n = 5$ ; 1 SD) with no obvious outliers, whereas the bedrock samples exhibit more scatter  
272 and are mostly older than the mean boulder age (Fig. 9).

273 Biorka Island, a small island off the western coast of central Baranof Island, was initially  
274 mapped as ice-covered throughout the LLGM (Dyke, 2004). Here, there are numerous ~1 m tall  
275 boulders that rise above the surrounding vegetation and rest on ice-sculpted bedrock. Vegetation  
276 and sediments mostly obscure underlying bedrock surfaces, and thus we only collected samples  
277 from boulders at this sampling site. Our four boulder samples yielded exposure ages of  $15.3 \pm$   
278  $0.5$  (18JB005; Fig. 4),  $14.9 \pm 0.6$  (18JB006),  $15.4 \pm 0.5$  (18JB007; Fig. 4), and  $13.7 \pm 0.5$  ka  
279 (18JB008), with a mean of  $14.8 \pm 0.8$  ka ( $n = 4$ ; 1 SD; Fig. 8).

280 We visited a summit ridge at 545 – 560 m asl on the western, ocean-facing side of  
281 northwestern Kruzof Island, previously mapped as ice-free throughout the LGM (Dalton et al.,

282 2020). There, we found many large stable boulders and exposed patches of glacially sculpted  
283 bedrock between vegetation exhibiting glacial grooves and chatter marks. Here, we sampled  
284 three large boulders ( $> 2 \times 2 \times 1$  m), which date to  $14.9 \pm 0.8$  (20SEAK-07; Fig. 4),  $14.9 \pm 0.9$   
285 (20SEAK-12) and  $14.6 \pm 0.8$  ka (20SEAK-13; Fig. 4), yielding a mean age of  $14.8 \pm 0.2$  ka ( $n =$   
286  $3$ ; 1 SD; Fig. 8). A bedrock surface at this site dates to  $13.4 \pm 1.0$  ka (20SEAK-10; Fig. 4) and  
287 sits  $\sim 10$  m below and  $\sim 10$  m away from the boulder that dated to  $14.6 \pm 0.8$  ka (20SEAK-13).

288 We collected samples from three sites on Chichagof Island (Chichagof Sites A – C; Fig.  
289 8). Unlike our other sampling locations which are on the ocean-facing, western sides of the  
290 archipelago, the Chichagof Island sites are all located inland. We visited these sites to determine  
291 the timing of ice retreat inland and to complement the findings of a previous study that  
292 documented ice withdrawal in the central and eastern Alexander Archipelago (Lesnek et al.,  
293 2020). Chichagof Island is notable for its relative lack of boulders – consequently, the boulders  
294 sampled here are smaller than those at other sites. While many bedrock outcrops featured smooth  
295 surfaces indicative of glacial erosion, we did not observe clear striations or chatter marks. At site  
296 A, a bedrock bench,  $^{10}\text{Be}$  ages from two small, perched boulders are  $12.7 \pm 0.7$  (20SEAK-15;  $0.5$   
297  $\times 0.3 \times 0.3$  m; 476 m asl; Fig. 4) and  $9.0 \pm 0.6$  ka (20SEAK-16;  $0.5 \times 0.4 \times 0.3$  m; 473 m asl). A  
298 quartz vein sampled from bedrock outcrop at this site has an exposure age of  $15.3 \pm 0.7$  ka  
299 (20SEAK-14). Site B is a series of bedrock ridges, and a single boulder yields an exposure age of  
300  $12.4 \pm 0.9$  ka (20SEAK-18; 817 m asl; Fig. 4), while an adjacent bedrock surface dates to  $14.1 \pm$   
301  $0.7$  ka (20SEAK-19; 816 m asl). Finally, site C is at the summit of a massif and one bedrock  
302 knob sampled here has an exposure age of  $17.7 \pm 0.8$  ka (20SEAK-22; 779 m asl; Fig. 4).

303

304

## 305 **5 Discussion**

306

### 307 **5.1 Bedrock $^{10}\text{Be}$ ages**

308

309 We sampled large and stable boulders in addition to bedrock surfaces with clear evidence  
310 of glacial erosion (e.g., striations, chatter marks) with the goal of providing optimal constraints  
311 on deglaciation. Sampling bedrock surfaces also allows us to better understand the subglacial  
312 erosion regime across the Alexander Archipelago, potentially yielding information about the  
313 duration of ice cover, the amount of subglacial erosion, and the likelihood of boulders containing  
314 inheritance.

315 Bedrock exposure ages are older than the mean boulder exposure ages by two SD or  
316 greater on Sumez Island (19SEAK-10) and Baranof sites A (19SEAK-18, 19SEAK-19) and D  
317 (19SEAK26, 19SEAK-27). At Chichagof site A the bedrock exposure age (20SEAK-14) is ~4.5  
318 kyr older than the mean boulder age, but still within two standard deviations, perhaps due to the  
319 large spread in boulder ages resulting in larger standard deviations. At Chichagof site B, the  
320 single boulder  $^{10}\text{Be}$  age (20SEAK-18) post-dates the single bedrock age by ~1.7 kyr. In general,  
321 bedrock data reported here are consistent with bedrock  $^{10}\text{Be}$  ages from Warren and Baker islands  
322 that are older (by more than 2 SD) than mean boulder ages (Lesnek et al., 2018). Bedrock ages  
323 may be erroneously older due to  $^{10}\text{Be}$  inheritance if ice sheet erosion was insufficient to remove  
324 the ~2 m of rock required to remove most of the previous  $^{10}\text{Be}$  inventory. Studies from British  
325 Columbia (Darvill et al., 2018) and Washington (Briner and Swanson, 1998) also report  
326 cosmogenic nuclide inheritance in bedrock from other areas covered by the Cordilleran Ice  
327 Sheet. In our field area, the short-lived nature of the overriding event (~3 kyr; Lesnek et al.,  
328 2018) may also contribute to the lack of significant glacial erosion. Finally, traces of inheritance

329 may be present in bedrock, perhaps even boulders, in ice-sheet-distal sites like these that are  
330 overrun by ice during extremely brief portions of the Quaternary (Briner et al., 2016).

331         In some cases, boulder-bedrock pairs have similar exposure ages (on southern Baranof  
332 and Suemez islands), suggesting our bedrock ages are unaffected by  $^{10}\text{Be}$  inheritance at these  
333 sites. On Kruzof Island, a bedrock patch yields an exposure age that is younger (by more than 2  
334  $\sigma$ ) than the mean age of the surrounding boulders. Potential cover by snow, sediment, or  
335 vegetation is thought to have caused anomalously young ages elsewhere in the Alexander  
336 Archipelago (Lesnek et al., 2020) and may also explain this  $^{10}\text{Be}$  age from our bedrock site on  
337 Kruzof Island.

338         Bedrock exposure ages vary greatly (by as much as  $\sim 14$  kyr) between the various  
339 sampling locations on Baranof Island and up to 6 kyr on Suemez Island (Lesnek et al., 2018).  
340 The Alexander Archipelago is characterized by impressive relief (deep fjords, high peaks), and  
341 thus, sub-glacial erosion rates clearly varied greatly across Suemez and Baranof islands where  
342 sampling locations are  $\sim 2 - 6$  km apart. Differing bedrock  $^{10}\text{Be}$  ages from the same sampling  
343 locales confirm this inference, reflecting variable sub-glacial erosion rates even within  $\sim 100$  m of  
344 each other. Some samples may have been collected in areas dominated by glacial abrasion,  
345 whereas other samples might be from surfaces dominated by quarrying, and thus, this variability  
346 could reflect varying subglacial processes on a local scale.

347         Because bedrock exposure ages from the coastal Alexander Archipelago (this study;  
348 Lesnek et al., 2018) do not consistently pre-date, match, or post-date exposure ages from  
349 adjacent boulders, we refrain from including bedrock-based  $^{10}\text{Be}$  ages in our mean deglaciation  
350 age calculations (Figs. 9; 10). This negates biases when choosing which bedrock ages “match”  
351 nearby erratic ages and allows us to eliminate any concern over inheritance or post-ice retreat

352 cover of these bedrock surfaces. While bedrock ages, especially when paired with boulder ages,  
353 are useful for identifying spatially variable subglacial erosion processes and issues with past  
354 cover and inheritance, they do not appear to provide reliable age constraints on the timing of  
355 deglaciation in the Alexander Archipelago due to the inconsistencies between bedrock and  
356 boulder ages. In light of this, we also recalculate relevant mean ages from Lesnek et al. (2018;  
357 2020) using solely boulder  $^{10}\text{Be}$  ages to update these other regional chronologies.

358

## 359 **5.2 $^{10}\text{Be}$ chronology incompatible with mapped Cordilleran Ice Sheet extent**

360

361 We targeted areas of the northern Alexander Archipelago mapped as ice-free by previous  
362 studies to determine whether these areas were LLGM refugia. The most recent coastal  
363 Cordilleran Ice Sheet reconstructions show significant portions of the northern Alexander  
364 Archipelago as remaining ice-free throughout the LLGM (Fig. 2), with ice terminating close to  
365 the present shoreline – not on the continental shelf (Dalton et al., 2020; Lesnek et al., 2020). Our  
366 data, however, indicate that at least some of these areas previously mapped as refugia  
367 (southwestern Baranof and Kruzof islands) were covered by ice, and deglaciated around 15.4 –  
368 14.8 ka. Our new evidence thus suggests that ice extended onto the continental shelf during the  
369 LLGM, as in the southern Alexander Archipelago (Lesnek et al., 2018). These discrepancies  
370 between previously mapped ice extents and those implied by our new exposure ages highlight  
371 the need to develop deglaciation chronologies elsewhere along the Cordilleran Ice Sheet coastal  
372 margin to provide updated mapping around the north Pacific.

373

374



### 375 **5.3 Cordilleran Ice Sheet retreat across the Alexander Archipelago**

376  
377 Mean boulder  $^{10}\text{Be}$  exposure ages from Suemez Island in this study and Lesnek et al.  
378 (2018),  $16. \pm 1.2$  ka ( $n = 3$  boulders; 1 SD) and  $16.6 \pm 0.8$  ka ( $n = 3$  boulders; 1 SD),  
379 respectively, overlap within 1 standard deviation (Figs. 6; 9). However, three of the boulder  $^{36}\text{Cl}$   
380 ages from southwestern Suemez Island do not overlap with the  $^{10}\text{Be}$  ages at 1 standard deviation  
381 (Figs. 6; 9). We attribute this scatter to post-depositional surface erosion of the basaltic boulders  
382 (i.e., those dated with  $^{36}\text{Cl}$ ) in excess of 3 mm/ka. Although we targeted areas of the boulder  
383 tops with no obvious signs of erosion, given the maritime climate of Southeast Alaska it is  
384 possible that the original, glacially eroded boulder surfaces have been weathered. Surface erosion  
385 of rocks with low concentrations of native Cl (supplementary table S2), where the primary  $^{36}\text{Cl}$   
386 production pathway is Ca-spallation (Marrero et al., 2016), results in exposure ages that are  
387 erroneously young. Thus, we interpret the oldest  $^{36}\text{Cl}$  exposure age ( $16.4 \pm 0.5$  ka; 19SEAK-02)  
388 as the closest constraint on deglaciation at that site. This  $^{36}\text{Cl}$  age overlaps with the  $^{10}\text{Be}$  ages  
389 from elsewhere on Suemez Island; we combine them and calculate a new, boulder-based mean  
390 deglaciation age of  $16.3 \pm 0.8$  ka ( $n = 10$  boulders; 1 SD) for Suemez Island.

391 We group together three of our sampling locations in the northern Alexander Archipelago  
392 that are ocean-facing: Kruzof, Biorka, and southern Baranof islands. As the Cordilleran Ice Sheet  
393 retreated from the continental shelf inland, these were the first areas presently above sea level to  
394 become ice-free. We calculate a mean  $^{10}\text{Be}$  boulder age of  $15.1 \pm 0.9$  ka ( $n = 12$  boulders; 1 SD)  
395 for the coastal northern Alexander Archipelago.

396 There are limited data from elsewhere in the northern Alexander Archipelago that  
397 constrain the timing of deglaciation. A basal pollen concentrate-based radiocarbon age from  
398 Hummingbird Lake (Fig. 7), southwestern Baranof Island dates to  $15.0 \pm 0.2$  cal ka, in

399 agreement with the  $^{10}\text{Be}$  ages presented here and that collectively indicate coastal Baranof Island  
400 was deglaciated prior to  $\sim 15$  ka (Ager, 2019). Additionally, tephra layers from Mt. Edgecumbe  
401 on Kruzof Island are dated to 13.1 ka (Riehle et al., 1992; Beget et al., 1998), and blanket many  
402 of the surrounding islands, suggesting that these areas were ice-free by then.

403 All three sample sites on Chichagof Island (Sites A – C) are not ocean-adjacent and  
404 characterized by a general lack of boulders. The boulders present were much smaller and shorter  
405 ( $< 0.5$  m high) than boulders sampled elsewhere across the Alexander Archipelago – we chose to  
406 sample these despite their size to provide minimum ages for deglaciation and to compare with  
407 available radiocarbon constraints. The ages of these boulders fall between  $9.0 \pm 0.6$  and  $12.7 \pm$   
408  $0.7$  ka and are thus younger than other age constraints for deglaciation on Chichagof Island;  
409 radiocarbon ages on shells from raised marine terraces on Chichagof Island date back to  $14.2 \pm$   
410  $0.6$  cal ka suggesting that the island was ice-free by this time (Baichtal et al., 2021). Smaller  
411 boulders are more susceptible to cover (whether snow, vegetation, or sediment), and may thus  
412 yield anomalously young  $^{10}\text{Be}$  ages. While a lack of large boulders found on Chichagof Island  
413 makes it difficult to ascertain the timing of deglaciation, regional glacial and sea-level history  
414 suggests Chichagof Island was deglaciated between 15.1 (when the coastal area deglaciated) and  
415 14.2 cal ka (the age of shells in raised marine deposits). Therefore, the boulders dated here likely  
416 have anomalously young exposure ages.

417 Our mean  $^{10}\text{Be}$  age of  $15.1 \pm 0.9$  ka ( $n = 12$  boulders; 1 SD) from all sites along the  
418 coastal portion of the northern Alexander Archipelago fits with the few other regional  
419 deglaciation constraints (Fig. 2) and overlaps within one standard deviation with the mean  
420 boulder exposure age from the southern Alexander Archipelago of  $16.3 \pm 0.8$  ka ( $n = 13$   
421 boulders; 1  $\sigma$ ; this study; Lesnek et al., 2018; Lesnek et al., 2020). While mean ages from the

422 northern and southern Alexander Archipelago overlap within one standard deviation, it is  
423 possible that these areas deglaciated at slightly different times as these various sampling sites  
424 happened to become ice-free. Furthermore, local ice caps formed and radiated from massifs on  
425 Chichagof, Baranof, and Prince of Wales islands during the LLGM (Capps, 1932; Mann and  
426 Hamilton, 1995; Lesnek et al., 2020). These local ice caps served as a local ice source for the  
427 Alexander Archipelago and their locations and flow patterns may have led to some parts of the  
428 archipelago becoming ice-free before others. Thus, we present a range of deglaciation across the  
429 coastal Alexander Archipelago from between  $16.3 \pm 0.8$  ka and  $15.1 \pm 0.9$  ka

430 Ice retreat across the Alexander Archipelago is also registered in marine sediments off  
431 the former coastal Cordilleran Ice Sheet margin. Several marine sedimentary records (cores  
432 EW0408-26JC, EW0408-66JC, EW0408-85JC) extending back to  $\sim 18.5$  cal ka show the  
433 presence of IRD beginning  $\sim 18.5$  ka, peaking at  $17.5 - 16.5$  ka and ceasing at  $14.8$  ka, reflecting  
434 a final retreat of marine-terminating ice (Praetorius and Mix, 2014). Furthermore, these IRD data  
435 record fluctuating but relatively elevated calving spanning  $18.5$  to  $14.8$  ka, perhaps indicating  
436 steady retreat punctuated by periods of accelerated melting.

437 Tephra from Mt. Edgecumbe (Kruzof Island) found in core EW0408-26JC is interpreted  
438 to have been deposited in a submarine environment, suggesting that this core site was ice-free by  
439  $14.6$  ka (Praetorius et al., 2016). Records of a subsequent eruption dated to  $\sim 13.1$  cal ka from  
440 marine sediments in Sitka Sound (core EW0408-40JC) indicate that this area (between Baranof  
441 and Kruzof islands) must have been ice-free by this time (Addison et al., 2010). Finally,  $^{14}\text{C}$  ages  
442 from mollusks found in a diamicton layer along the Gastineau Channel date to  $\sim 13.8$  cal ka,  
443 reflecting the beginning of deglaciation near the mainland (Miller, 1973; we calibrate all  
444 uncalibrated  $^{14}\text{C}$  ages with CALIB 8.2; Stuiver et al., 2021).

#### 445 **5.4 Chronologies of Cordilleran Ice Sheet deglaciation across the North Pacific**

446  
447 Radiocarbon ages from the Cordilleran Ice Sheet margin reflect ice advance from ~20 –  
448 17 ka, near the end of the GLGM at 19 ka. Ages from mammalian fossils in Shuká Káa on Prince  
449 of Wales Island indicate Cordilleran Ice Sheet advance ~20 ka in the Alexander Archipelago  
450 (Lesnek et al., 2018). Directly south of the Alexander Archipelago, on eastern Graham Island  
451 (Haida Gwaii) initial ice advance is dated to 24.1 – 22.5 cal ka with a <sup>14</sup>C date from a twig  
452 underlying till (Blaise et al., 1990; Mathewes and Clague, 2017). Along the southwestern  
453 Cordilleran Ice Sheet margin, ice reached its maximum extent until ~17.0 ka in the Puget Sound  
454 area (Porter and Swanson, 1998).

455 Glacier chronologies from the northeastern Pacific coastline also reflect post-GLGM  
456 retreat. On Sanak Island, tephra near the bottom of a lake sediment core dates deglaciation before  
457 ~15.9 ka, broadly synchronous with Cordilleran Ice Sheet withdrawal in the Alexander  
458 Archipelago (Misarti et al., 2012). On Kodiak Island, final LLGM retreat dates to ~15.7 cal ka,  
459 as marked by a <sup>14</sup>C age above glacio-tectonically altered sediments (Mann and Peteet, 1994).  
460 Directly north of the Alexander Archipelago, a <sup>14</sup>C age from a log found within the Finger  
461 Glacier lateral moraine provides a minimum age of deglaciation at ~14.6 cal ka (Mann, 1986).  
462 Radiocarbon ages from a marine sediment core in Dixon Entrance date maximum Cordilleran Ice  
463 Sheet extent to before ~16.1 cal ka and retreat beginning before ~15.3 cal ka (Barrie and  
464 Conway, 1999). A marine sediment record from Vancouver Sound similarly dates maximum ice  
465 extent to 18.5 ka and retreat of the Cordilleran Ice Sheet onto the mainland by 16.4 ka (Blaise et  
466 al., 1990). Quaternary sediments on eastern Graham Island indicate the Cordilleran Ice Sheet was  
467 retreating by 17.8 cal ka (Blaise et al., 1990). Notably, <sup>10</sup>Be ages on Calvert Island suggest ice

468 retreated off the continental shelf at ~18 ka, pre-dating ice withdrawal onto land in the Alexander  
469 Archipelago (Darvill et al., 2018).

470 Marine sediment cores are interpreted to show ice retreat across the coastal northeastern  
471 Pacific. A marine sediment core (SO202-27-6) from the Gulf of Alaska captures a decrease in  
472 sea surface salinity ~16 ka, interpreted to reflect increased meltwater from the Cordilleran Ice  
473 Sheet margin (Maier et al., 2018). Another marine sediment core (EW0408-85JC) recovered off  
474 the coast of southern Alaska records a decrease in glacial-margin sediment accumulation at 16.9  
475 ka as ice stagnated or began to retreat. (Davies et al., 2011). Reductions in salinity captured by  
476 planktonic  $\delta^{18}\text{O}$  in this core at ~16.7 ka are interpreted as an increase in meltwater input from  
477 retreating glaciers. A transition from ice-proximal to laminated hemipelagic sediments at ~14.8  
478 ka marks glacier retreat off the continental shelf and onto land. Off the coast of Alaska, a marine  
479 sediment core records a peak of IRD deposition peaking between 18 and 17 ka, interpreted as the  
480 retreat of marine-terminating margins of the Cordilleran Ice Sheet (Walczak et al., 2020).  
481 Additionally, another core from off Vancouver Island (MD02-2496) captures IRD deposition  
482 between ~17.0 and ~16.2 cal ka – indicating rapid regional deglaciation – and a minor IRD event  
483 at ~14.7 cal ka (Cosma et al., 2008).

484 Our new data showing ice retreat at  $15.1 \pm 0.9$  ka from the northern Alexander  
485 Archipelago, along with ages of deglaciation from the southern Alexander Archipelago ( $16.3 \pm$   
486  $0.8$  ka; this study; Lesnek et al., 2018), are broadly synchronous with previously published ice  
487 retreat chronologies for the marine-terminating Cordilleran Ice Sheet margin elsewhere along the  
488 northeast Pacific Coast. However, while our chronology only documents deglaciation, it provides  
489 further evidence of a delayed LLGM across the coastal Cordilleran Ice Sheet compared to the

490 GLGM maximum extents of alpine glaciers in mainland Alaska (Briner et al., 2017), parts of  
491 southern Alaska (Reger et al., 1996), and the Laurentide Ice Sheet (Dalton et al., 2020).

492

### 493 **5.5 Paleoclimate Records from the North Pacific**

494

495         Several paleoclimate records from around the North Pacific span our interval of  
496 Cordilleran Ice Sheet deglaciation in the Alexander Archipelago. A combined diatom  
497 assemblage- and alkenone-derived record of sea surface temperatures (SSTs) from the Bering  
498 Sea (Core 51JPC), records perennial sea ice from ~22.5 ka (beginning of record) to 17 ka, and  
499 increased SSTs beginning ~16.9 ka before a notable shift back to annual sea ice ~16.7 ka  
500 (Caissie et al., 2010). In the northern Gulf of Alaska (Core EW0408-85JC),  $\delta^{18}\text{O}$  data document  
501 increasing SSTs at 16.7 ka and again at ~14.7 ka (Davies et al., 2011). Alkenone-inferred paleo-  
502 SST reconstructions from this same core show the lowest SSTs (~5 °C) circa 17.0 ka, with  
503 increased SSTs beginning ~16.5 ka, and a rapid ~3 - 4 °C rise in SSTs from 15.2 to 14.7 ka  
504 (Praetorius et al., 2015). Alkenone-inferred SST and  $\delta^{18}\text{O}$  records from the Gulf of Alaska also  
505 record increased SSTs of ~3°C at 14.7 ka (cores EW0408-26JC, EW0408-66JC; Praetorius et al.,  
506 2016). Off Vancouver Island, Mg/Ca temperature reconstructions from subsurface-dwelling *N.*  
507 *pachyderma* indicate two stages of warming of ~2 °C at 17.2 – 16 ka, and a further ~3 °C 15.5 –  
508 14.0 ka, while surface-dwelling *G. bulloides* record a 3 °C SST increase from 15.0 – 14.0 ka  
509 (core MD02-2496; Taylor et al., 2014), all within the uncertainty of coastal Alexander  
510 Archipelago ice retreat. Alkenone SST reconstructions from another nearby core (core JT96-09)  
511 also indicates a 4 °C increase in SST at ~14.7 ka (Kienast and McKay, 2001).

512         There are few terrestrial paleoclimate data that span the last deglacial period from  
513 southeast Alaska and coastal British Columbia. Cordilleran ice cover until ~15 ka across much of

514 the region impeded the preservation of many terrestrial records – however, there are limited ice  
515 core, speleothem, and lake records that date back to early regional deglaciation or prior. A  
516 growth hiatus in a speleothem from El Capitan Cave (southern Alexander Archipelago) spanning  
517 ~41.5 to ~13.4 ka suggests the cave was either overridden by the Cordilleran Ice Sheet,  
518 experienced permafrost conditions and a mean annual air temperature  $< 0\text{ }^{\circ}\text{C}$ , or lacked drip  
519 water (Wilcox et al., 2019). The youngest date also serves as a minimum limit on deglaciation, as  
520 the area was thawed by ~13.4 ka. However, El Capitan Cave is ~60 km inland of the outermost  
521 coastal region and therefore may have still experienced these conditions while the outer coast  
522 deglaciated. At Hummingbird Lake, southwestern Baranof Island, pollen records indicate *Pinus*  
523 *contorta* dominated from ~15.2 ka to 14 ka, which is interpreted to represent *Pinus contorta*  
524 response to the beginnings of Gulf of Alaska ocean warming at ~16.5 ka (Praetorius et al., 2015;  
525 Ager, 2019). This record suggests increased air temperatures around deglaciation of the  
526 Alexander Archipelago between  $16.3 \pm 0.8$  ka and  $15.1 \pm 0.9$  ka.

527

## 528 **5.6 Implications for early human migration**

529

530 Several studies have scrutinized potential areas of LLGM glacial refugia in the Alexander  
531 Archipelago through a human migration perspective (Carrara et al., 2007; Lesnek et al., 2018),  
532 building off similar approaches from elsewhere in the North Pacific (e.g., Warner et al., 1982;  
533 Mann and Peteet, 1994; Misarti et al., 2012). Our study focused on southern Baranof and Kruzof  
534 islands because previous mapping suggested that parts of these areas were ice-free throughout  
535 the LLGM (Carrara et al., 2003; Carrara et al., 2007). However, our  $^{10}\text{Be}$  ages from southern  
536 Baranof Island indicate these areas were glaciated throughout the LLGM and not available for

537 human habitation between ~20 ka and ~15.4 ka. Our exposure ages from Kruzof Island also  
538 suggest this area was not ice free until ~14.8 ka.

539         These results indicate that some of the last major unevaluated areas of possible refugia  
540 presently above sea-level were covered by ice during the LLGM. At its maximum extent, ice  
541 likely extended onto the then-exposed continental shelf. Ice occupation of the continental shelf –  
542 or at least parts of the shelf – off the Alexander Archipelago was relatively brief, from ~20.0 to  
543 ~16.0 ka (Lesnek et al., 2018). Areas of the continental shelf would have been above modern sea  
544 level during this time and until ~11 – 8 ka, when sea level neared modern levels in the Alexander  
545 Archipelago (Baichtal et al., 2021). At a minimum, ice lobes would have existed within the  
546 major shelf troughs (e.g., Chatham Strait), likely crossing the entire shelf at these locations; at a  
547 maximum, the entire continental shelf may have been occupied by ice from ~20 to ~16 ka.  
548 Whether portions of the shelf remained ice-free during the LLGM is unknown, but it is possible.  
549 Based on the immediate colonization of *Pinus* at 15.2 ka in Hummingbird Lake and as early as  
550 ~15.4 ka on Pleasant Island, there were likely ice-free areas on the shelf throughout the LLGM  
551 (Hansen and Engstrom, 1996; Ager, 2019).

552

## 553 **6 Conclusions**

554

555         We conclude that several areas in southeast Alaska previously mapped as ice-free  
556 through the LLGM were covered by ice until between ~16.3 and ~15.1 ka. <sup>10</sup>Be ages from  
557 boulders suggest that the northern coastal Alexander Archipelago deglaciated at  $15.1 \pm 0.9$  ka,  
558 while <sup>10</sup>Be and <sup>36</sup>Cl ages date ice retreat in the southern portion at  $16.3 \pm 0.8$  ka, following a  
559 LLGM that began after ~20 ka (Lesnek et al., 2018; Lesnek et al., 2020) The timing of  
560 deglaciation in the Alexander Archipelago is similar to some other sites around the Cordilleran



561 Ice Sheet coastal margin (e.g., Mann and Peteet, 1994; Misarti et al., 2012), but later than other  
562 locations (e.g., Darvill et al., 2018). Notably, the deglaciation in southeast Alaska is later than in  
563 mainland Alaska and Kodiak and Sanak Islands, Alaska (Fig. 1), where records are more aligned  
564 with the GLGM. The timing of deglaciation in the Alexander Archipelago is broadly  
565 synchronous with regional records of local ocean and air temperature increases. We also found  
566 that anomalously old  $^{10}\text{Be}$  ages of bedrock surfaces are likely due to inheritance caused by  
567 insufficient ice sheet erosion, and thus urge caution when using ages from bedrock surfaces as  
568 direct constraints on ice retreat without additional boulder ages along the coastal margins of the  
569 Cordilleran Ice Sheet.

570 Our data indicate that previous mapping of the coastal Cordilleran Ice Sheet can be  
571 spatially and temporally improved. We suggest that ice likely extended out on the continental  
572 shelf along the Alexander Archipelago. We are increasingly confident that areas of the coastal  
573 Cordilleran Ice Sheet previously mapped as ice-free throughout the LLGM were in fact covered  
574 by ice, and that refugia, if any existed, would have been located on the exposed continental shelf.  
575 Although more logistically challenging, subsequent studies should evaluate the existence of  
576 LLGM refugia in the Alexander Archipelago by focusing on the previously exposed continental  
577 shelf. Special attention should be given to the northern Alexander Archipelago where ice masses  
578 were fed by local ice caps and thus may not have been as extensive, as opposed to elsewhere in  
579 the northeastern Pacific where ice was sourced from the main body of the Cordilleran Ice Sheet.

580

## 581 **7 Acknowledgements**

582

583 We acknowledge that these samples were collected on the ancestral lands of the Tlingit  
584 and that the University at Buffalo exists on the land of the Seneca. These peoples are the

585 traditional caretakers of these lands and we give thanks for the opportunity to exist and work on  
586 lands that are rightfully theirs. We thank the Tongass National Forest for assistance with  
587 permitting and logistics. We thank Corey Krabbenhoft, Joseph Tulenko and Karlee Prince for  
588 field assistance and Joseph Tulenko and Chris Sbarra for lab assistance. We also thank PRIME  
589 Lab for  $^{10}\text{Be}$  measurements and Lawrence Livermore National Laboratory for  $^{36}\text{Cl}$   
590 measurements. This research was funded by NSF (award # 1854550), the National Geographic  
591 Society (award # 57989R-19), a Geological Society of America Student Research Grant (grant  
592 number 13631) funded by NSF (award # 1949901), the Alaska Geological Society, and the Mark  
593 Diamond Research Fund of the Graduate Student Association at the University at Buffalo, the  
594 State University of New York.

595

## 596 **8 Author Contributions**

597 JPB designed the study framework and acquired the majority of grant funds. CKW acquired  
598 supplementary funding for fieldwork and lab analyses. CKW, JPB, JFB, and AJL collected  
599 samples in the field. CKW conducted  $^{10}\text{Be}$  work and AJL and JML performed  $^{36}\text{Cl}$  chemistry.  
600 CKW, JPB, AJL, and JML analyzed sample data and calculated ages. All authors were involved  
601 in interpreting the data. CKW wrote the first draft of the manuscript; all authors provided  
602 substantial input. CKW and AJL created figures and tables.

603

604

605

606

607

608 **9 References**

- 609
- 610 Addison, J. A., Beget, J. E., Ager, T. A., and Finney, B. P.: Marine tephrochronology of the Mt.  
611 Edgumbe volcanic field, southeast Alaska, USA, *Quaternary Research*, 73, 277-292,  
612 2010.
- 613 Ager, T. A.: Late Quaternary vegetation development following deglaciation of northwestern  
614 Alexander Archipelago, Alaska, *Frontiers in Earth Science*, 7, 104, 2019.
- 615 Baichtal, J. F., Lesnek, A. J., Carlson, R. J., Schmuck, N., Smith, J. L., Landwehr, D. J., and  
616 Briner, J. P.: Late Pleistocene and Early Holocene Sea level History Glacial Retreat  
617 Interpreted from Shell-bearing Marine Deposits of Southeastern Alaska, *GSA Geosphere*,  
618 2021.
- 619 Balco, G., Stone, J. O., Lifton, N. A., and Dunai, T. J.: A complete and easily accessible means  
620 of calculating surface exposure ages or erosion rates from  $^{10}\text{Be}$  and  $^{26}\text{Al}$  measurements,  
621 *Quaternary Geochronology*, 3, 174-195, <https://doi.org/10.1016/j.quageo.2007.12.001>,  
622 2008.
- 623 Balco, G.: Production rate calculations for cosmic-ray-muon-produced  $^{10}\text{Be}$  and  $^{26}\text{Al}$   
624 benchmarked against geological calibration data, *Quaternary Geochronology*, 39, 150-  
625 173, 2017.
- 626 Barrie, J. V., and Conway, K. W.: Late Quaternary glaciation and postglacial stratigraphy of the  
627 northern Pacific margin of Canada, *Quaternary Research*, 51, 113-123, 1999.
- 628 Begét, J. E. and Motyka, R. J.: New dates on late Pleistocene dacitic tephra from the Mount  
629 Edgumbe volcanic field, southeastern Alaska, *Quaternary Research*, 49, 123-125, 1998.
- 630 Blaise, B., Clague, J. J., and Mathewes, R. W.: Time of maximum Late Wisconsin glaciation,  
631 West Coast of Canada, *Quaternary Research*, 34, 282-295, [https://doi.org/10.1016/0033-](https://doi.org/10.1016/0033-5894(90)90041-I)  
632 [5894\(90\)90041-I](https://doi.org/10.1016/0033-5894(90)90041-I), 1990.
- 633 Booth, D. B., Troost, K. G., Clague, J. J., and Waitt, R. B.: The Cordilleran ice sheet,  
634 *Developments in Quaternary Sciences*, 1, 17-43, 2003.
- 635 Borchers, B., Marrero, S., Balco, G., Caffee, M., Goehring, B., Lifton, N., Nishiizumi, K.,  
636 Phillips, F., Schaefer, J., and Stone, J. J. Q. G.: Geological calibration of spallation  
637 production rates in the CRONUS-Earth project, 31, 188-198, 2016.
- 638 Brew, David A.: Geologic map of the Craig, Dixon Entrance, and parts of the Ketchikan and  
639 Prince Rupert quadrangles, Southeastern Alaska, No. 95-215, 1995.
- 640 Briner, J. P., and Swanson, T. W.: Using inherited cosmogenic  $^{36}\text{Cl}$  to constrain glacial erosion  
641 rates of the Cordilleran ice sheet, *Geology*, 26, 3-6, 1998.
- 642 Briner, J. P., Goehring, B. M., Mangerud, J., and Svendsen, J. I.: The deep accumulation of  $^{10}\text{Be}$   
643 at Utsira, southwestern Norway: implications for cosmogenic nuclide exposure dating in  
644 peripheral ice sheet landscapes, *Geophysical Research Letters*, 43, 9121-9129, 2016.
- 645 Briner, J. P., Tulenko, J. P., Kaufman, D. S., Young, N. E., Baichtal, J. F., and Lesnek, A.: The  
646 last deglaciation of Alaska, *Cuadernos de investigación geográfica/Geographical*  
647 *Research Letters*, 429-448, 2017.
- 648 Caissie, B. E., Brigham-Grette, J., Lawrence, K. T., Herbert, T. D., and Cook, M. S.: Last Glacial  
649 Maximum to Holocene sea surface conditions at Umnak Plateau, Bering Sea, as inferred  
650 from diatom, alkenone, and stable isotope records, *Paleoceanography*, 25, 2010.
- 651 Capps, S. R.: *Glaciation in Alaska, 2330-7102, 1932.*

- 652 Carrara, P. E., Ager, T. A., Baichtal, J. F., and VanSistine, D. P.: Map of glacial limits and  
653 possible refugia in the southern Alexander Archipelago, Alaska, during the late  
654 Wisconsin glaciation, Report 2424, 2003.
- 655 Carrara, P. E., Ager, T. A., and Baichtal, J. F.: Possible refugia in the Alexander Archipelago of  
656 southeastern Alaska during the late Wisconsin glaciation, *Canadian Journal of Earth  
657 Sciences*, 44, 229-244, 10.1139/e06-081, 2007.
- 658 Cook, J. A., Bidlack, A. L., Conroy, C. J., Demboski, J. R., Fleming, M. A., Runck, A. M.,  
659 Stone, K. D., and MacDonald, S. O.: A phylogeographic perspective on endemism in the  
660 Alexander Archipelago of southeast Alaska, *Biological Conservation*, 97, 215-227,  
661 [https://doi.org/10.1016/S0006-3207\(00\)00114-2](https://doi.org/10.1016/S0006-3207(00)00114-2), 2001.
- 662 Corbett, L. B., Bierman, P. R., and Rood, D. H.: An approach for optimizing in situ cosmogenic  
663 <sup>10</sup>Be sample preparation, *Quaternary Geochronology*, 33, 24-34,  
664 <https://doi.org/10.1016/j.quageo.2016.02.001>, 2016.
- 665 Cosma, T. N., Hendy, I. L., and Chang, A. S.: Chronological constraints on Cordilleran Ice Sheet  
666 glaciomarine sedimentation from core MD02-2496 off Vancouver Island (western  
667 Canada), *Quaternary Science Reviews*, 27, 941-955,  
668 <https://doi.org/10.1016/j.quascirev.2008.01.013>, 2008.
- 669 Dalton, A. S., Margold, M., Stokes, C. R., Tarasov, L., Dyke, A. S., Adams, R. S., Allard, S.,  
670 Arends, H. E., Atkinson, N., and Attig, J. W.: An updated radiocarbon-based ice margin  
671 chronology for the last deglaciation of the North American Ice Sheet Complex,  
672 *Quaternary Science Reviews*, 234, 106223, 2020.
- 673 Darvill, C. M., Menounos, B., Goehring, B. M., Lian, O. B., and Caffee, M. W.: Retreat of the  
674 western Cordilleran ice sheet margin during the last deglaciation, *Geophysical Research  
675 Letters*, 45, 9710-9720, 2018.
- 676 Davies, M. H., Mix, A. C., Stoner, J. S., Addison, J. A., Jaeger, J., Finney, B., and Wiest, J.: The  
677 deglacial transition on the southeastern Alaska Margin: Meltwater input, sea level rise,  
678 marine productivity, and sedimentary anoxia, *Palaeogeography and Palaeoclimatology*,  
679 26, 10.1029/2010pa002051, 2011.
- 680 Demboski, J. R., Stone, K. D., and Cook, J. A.: Further perspectives on the Haida Gwaii glacial  
681 refugium, *Evolution*, 53, 2008-2012, 10.1111/j.1558-5646.1999.tb04584.x, 1999.
- 682 Dyke, A. S.: An outline of North American deglaciation with emphasis on central and northern  
683 Canada, *Developments in quaternary sciences*, 2, 373-424, 2004.
- 684 Eberlein, G. D., Churkin, M., Carter, C., Berg, H., and Ovenshine, A.: *Geology of the Craig  
685 quadrangle, Alaska*, US Geological Survey, 2331-1258, 1983.
- 686 Faure, G.: Isotope systematics in two-component mixtures, *Principles of isotope geology*, 141-  
687 153, 1986.
- 688 Gosse, J. C., and Phillips, F. M.: Terrestrial in situ cosmogenic nuclides: theory and application.  
689 *Quaternary Science Reviews*, 20, 1475-1560, 2001.
- 690 Gregoire, L. J., Otto-Bliesner, B., Valdes, P. J., and Ivanovic, R.: Abrupt Bølling warming and  
691 ice saddle collapse contributions to the Meltwater Pulse 1a rapid sea level rise,  
692 *Geophysical research letters*, 43, 9130-9137, 2016.
- 693 Hansen, B. C. S., and Engstrom, D. R.: Vegetation history of Pleasant Island, southeastern  
694 Alaska, since 13,000 yr BP, *Quaternary Research*, 46, 161-175, 1996.
- 695 Hebda, C. F. G., McLaren, D., Mackie, Q., Fedje, D., Pedersen, M. W., Willerslev, E., Brown,  
696 K.J., and Hebda, R. J.: Late Pleistocene palaeoenvironments and a possible glacial  
697 refugium on northern Vancouver Island, Canada: Evidence for the viability of early

- 698 human settlement on the northwest coast of North America, *Quaternary Science Reviews*,  
699 279, 107388, 2022.
- 700 Ivanovic, R. F., Gregoire, L. J., Wickert, A. D., Valdes, P. J., and Burke, A.: Collapse of the  
701 North American ice saddle 14,500 years ago caused widespread cooling and reduced  
702 ocean overturning circulation, *Geophysical Research Letters*, 44, 383-392, 2017.
- 703 Jones, R. S., Whitehouse, P. L., Bentley, M. J., Small, D., and Dalton, A. S.: Impact of glacial  
704 isostatic adjustment on cosmogenic surface-exposure dating, *Quaternary Science  
705 Reviews*, 212, 206-212, 2019.
- 706 Kienast, S. S., and McKay, J. L.: Sea surface temperatures in the subarctic northeast Pacific  
707 reflect millennial-scale climate oscillations during the last 16 kyrs, *Geophysical Research  
708 Letters*, 28, 1563-1566, 2001.
- 709 Lal, D.: Cosmic ray labeling of erosion surfaces: in situ nuclide production rates and erosion  
710 models, *Earth and Planetary Science Letters*, 104, 424-439, 1991.
- 711 Lesnek, A. J., Briner, J. P., Lindqvist, C., Baichtal, J. F., and Heaton, T. H.: Deglaciation of the  
712 Pacific coastal corridor directly preceded the human colonization of the Americas,  
713 *Science Advances*, 4, 2018.
- 714 Lesnek, A. J., Briner, J. P., Baichtal, J. F., and Lyles, A. S.: New constraints on the last  
715 deglaciation of the Cordilleran Ice Sheet in coastal Southeast Alaska, *Quaternary  
716 Research*, 96, 140-160, 2020.
- 717 Maier, E., Zhang, X., Abelmann, A., Gersonde, R., Mulitza, S., Werner, M., Méheust, M., Ren,  
718 J., Chaplignin, B., and Meyer, H.: North Pacific freshwater events linked to changes in  
719 glacial ocean circulation, *Nature*, 559, 241-245, 2018.
- 720 Mann, D. H.: Wisconsin and Holocene glaciation of southeast Alaska, 1986.
- 721 Mann, D. H., and Peteet, D. M.: Extent and Timing of the Last Glacial Maximum in  
722 Southwestern Alaska, *Quaternary Research*, 42, 136-148,  
723 <https://doi.org/10.1006/qres.1994.1063>, 1994.
- 724 Mann, D. H., and Hamilton, T. D.: Late Pleistocene and Holocene Paleoenvironments of the  
725 Pacific Coast, *Quaternary Science Reviews*, 14, 449-471, 10.1016/0277-3791(95)00016-  
726 i, 1995.
- 727 Marrero, S.M., Phillips, F.M., Caffee, M.W. and Gosse, J.C.: CRONUS-Earth cosmogenic <sup>36</sup>Cl  
728 calibration. *Quaternary Geochronology*, 31, 199-219, 2016.
- 729 Menounos, B., Goehring, B. M., Osborn, G., Margold, M., Ward, B., Bond, J., Clarke, G. K. C.,  
730 Clague, J. J., Lakeman, T., Koch, J., Caffee, M. W., Gosse, J., Stroeven, A. P., Seguinot,  
731 J., and Heyman, J.: Cordilleran Ice Sheet mass loss preceded climate reversals near the  
732 Pleistocene Termination, *Science*, 358, 781, 10.1126/science.aan3001, 2017.
- 733 Mathewes, R. W., and Clague, J. J.: Paleoecology and ice limits of the early Fraser glaciation  
734 (Marine Isotope Stage 2) on Haida Gwaii, British Columbia, Canada, *Quaternary  
735 Research*, 88, 277-292, 10.1017/qua.2017.36, 2017.
- 736 Miller, R. D.: Gastineau channel formation: a composite glaciomarine deposit near Juneau,  
737 Alaska, US Government Printing Office, 1973.
- 738 Misarti, N., Finney, B. P., Jordan, J. W., Maschner, H. D. G., Addison, J. A., Shapley, M. D.,  
739 Krumhardt, A., and Beget, J. E.: Early retreat of the Alaska Peninsula Glacier Complex  
740 and the implications for coastal migrations of First Americans, *Quaternary Science  
741 Reviews*, 48, 1-6, <https://doi.org/10.1016/j.quascirev.2012.05.014>, 2012.
- 742 Molnia, B. F.: *Glaciers of North America-Glaciers of Alaska*, Geological Survey (US), 2008.

- 743 Nishiizumi, K., Imamura, M., Caffee, M. W., Southon, J. R., Finkel, R. C., and McAninch, J.:  
744 Absolute calibration of  $^{10}\text{Be}$  AMS standards, *Nuclear Instruments and Methods in*  
745 *Physics Research Section B: Beam Interactions with Materials and Atoms*, 258, 403-413,  
746 <https://doi.org/10.1016/j.nimb.2007.01.297>, 2007.
- 747 Porter, S. C., and Swanson, T. W.: Radiocarbon age constraints on rates of advance and retreat of  
748 the Puget lobe of the Cordilleran ice sheet during the last glaciation, *Quaternary*  
749 *Research*, 50, 205-213, 1998.
- 750 Praetorius, S. K., and Mix, A. C.: Synchronization of North Pacific and Greenland climates  
751 preceded abrupt deglacial warming, *Science*, 345, 444-448, 2014.
- 752 Praetorius, S. K., Mix, A. C., Walczak, M. H., Wolhowe, M. D., Addison, J. A., and Prah, F. G.:  
753 North Pacific deglacial hypoxic events linked to abrupt ocean warming, *Nature*, 527,  
754 362-366, 2015.
- 755 Praetorius, S., Mix, A., Jensen, B., Froese, D., Milne, G., Wolhowe, M., Addison, J., and Prah, F.:  
756 Interaction between climate, volcanism, and isostatic rebound in Southeast Alaska  
757 during the last deglaciation, *Earth and Planetary Science Letters*, 452, 79-89, 2016.
- 758 Reger, R. D., Pinney, D. S., Burke, R. M., and Wiltse, M. A.: Catalog and initial analyses of  
759 geologic data related to middle to late Quaternary deposits, Cook Inlet region, Alaska,  
760 State of Alaska Division of Geological and Geophysical Surveys Report of  
761 Investigations, 95-96, 1996.
- 762 Riehle, J. R., Brew, D. A., Reed, K. M., and Bartsch-Winkler, S.: Explosive latest Pleistocene (?)  
763 and Holocene activity of the Mount Edgecumbe volcanic field, Alaska, *US Geological*  
764 *Survey Circular*, 939, 111-114, 1984.
- 765 Riehle, J. R., Champion, D. E., Brew, D. A., and Lanphere, M. A.: Pyroclastic deposits of the  
766 Mount Edgecumbe volcanic field, southeast Alaska: eruptions of a stratified magma  
767 chamber, *Journal of volcanology and geothermal research*, 53, 117-143, 1992.
- 768 Riehle, J. R.: The Mount Edgecumbe Volcanic Field: A Geologic History, US Department of  
769 Agriculture, Forest Service, Alaska Region, 1996.
- 770 Seguinot, J., Khroulev, C., Rogozhina, I., Stroeven, A. P., and Zhang, Q.: The effect of climate  
771 forcing on numerical simulations of the Cordilleran ice sheet at the Last Glacial  
772 Maximum, *The Cryosphere*, 8, 1087-1103, 2014.
- 773 Seguinot, J., Rogozhina, I., Stroeven, A. P., Margold, M., and Kleman, J.: Numerical simulations  
774 of the Cordilleran ice sheet through the last glacial cycle, *The Cryosphere*, 10, 639-664,  
775 2016.
- 776 Shafer, A. B., Cullingham, C. I., Cote, S. D., and Coltman, D. W.: Of glaciers and refugia: a  
777 decade of study sheds new light on the phylogeography of northwestern North America,  
778 *Mol Ecol*, 19, 4589-4621, [10.1111/j.1365-294X.2010.04828.x](https://doi.org/10.1111/j.1365-294X.2010.04828.x), 2010.
- 779 Shafer, A. B. A., White, K. S., Côté, S. D., and Coltman, D. W.: Deciphering translocations from  
780 relicts in Baranof Island mountain goats: is an endemic genetic lineage at risk?,  
781 *Conservation Genetics*, 12, 1261-1268, [10.1007/s10592-011-0227-8](https://doi.org/10.1007/s10592-011-0227-8), 2011.
- 782 Shakun, J. D., Clark, P. U., He, F., Marcott, S. A., Mix, A. C., Liu, Z., Otto-Bliesner, B.,  
783 Schmittner, A., and Bard, E.: Global warming preceded by increasing carbon dioxide  
784 concentrations during the last deglaciation, *Nature*, 484, 49-54, 2012.
- 785 Spratt, R. M., and Lisiecki, L. E.: A Late Pleistocene sea level stack, *Climate of the Past*, 12,  
786 1079-1092, 2016.

- 787 Staiger, J., Gosse, J., Toracinta, R., Oglesby, B., Fastook, J., and Johnson, J. V.: Atmospheric  
788 scaling of cosmogenic nuclide production: climate effect, *Journal of Geophysical*  
789 *Research: Solid Earth*, 112, 2007.
- 790 Stuiver, M., Reimer, P.J., and Reimer, R.W., CALIB 8.2, <http://calib.org>, 2021.
- 791 Tarasov, L., Dyke, A. S., Neal, R. M., and Peltier, W. R.: A data-calibrated distribution of  
792 deglacial chronologies for the North American ice complex from glaciological modeling,  
793 *Earth and Planetary Science Letters*, 315-316, 30-40,  
794 <https://doi.org/10.1016/j.epsl.2011.09.010>, 2012.
- 795 Taylor, M. A., Hendy, I. L., and Pak, D. K.: Deglacial ocean warming and marine margin retreat  
796 of the Cordilleran Ice Sheet in the North Pacific Ocean, *Earth and Planetary Science*  
797 *Letters*, 403, 89-98, 10.1016/j.epsl.2014.06.026, 2014.
- 798 Warner, B. G., Mathewes, R. W., and Clague, J. J.: Ice-free conditions on the Queen Charlotte  
799 Islands, British Columbia, at the height of late Wisconsin glaciation, *Science*, 218, 675-  
800 677, 1982.
- 801 Wilcox, P. S., Dorale, J. A., Baichtal, J. F., Spotl, C., Fowell, S. J., Edwards, R. L., and Kovarik,  
802 J. L.: Millennial-scale glacial climate variability in Southeastern Alaska follows  
803 Dansgaard-Oeschger cyclicality, *Sci Rep*, 9, 7880, 10.1038/s41598-019-44231-1, 2019.
- 804 Wilson, F. H., Hults, C. P., Mull, C. G., and Karl, S. M.: Geologic map of Alaska, US  
805 Department of the Interior, US Geological Survey, 2015.
- 806 Young, N. E., Schaefer, J. M., Briner, J. P., and Goehring, B. M.: A  $^{10}\text{Be}$  production-rate  
807 calibration for the Arctic, *Journal of Quaternary Science*, 28, 515-526, 2013.

808

809

810

811

812

813

814

815

816

817

818

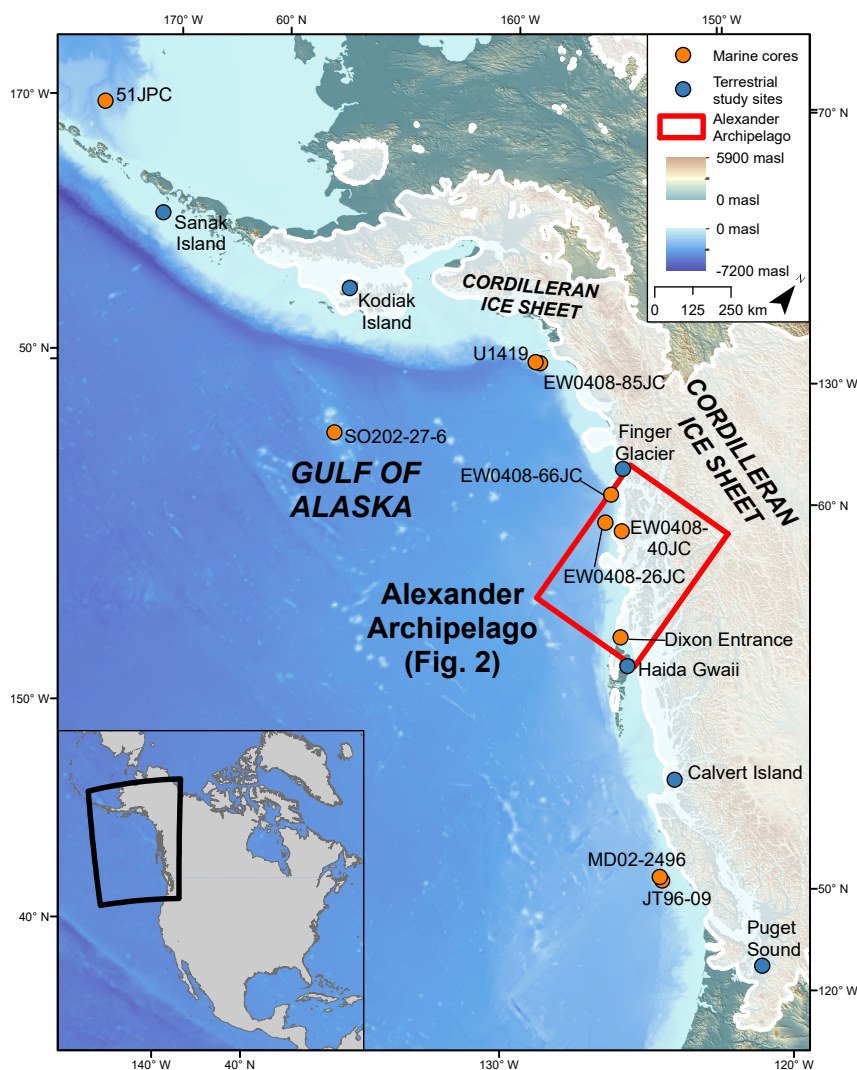
819

820

821

822

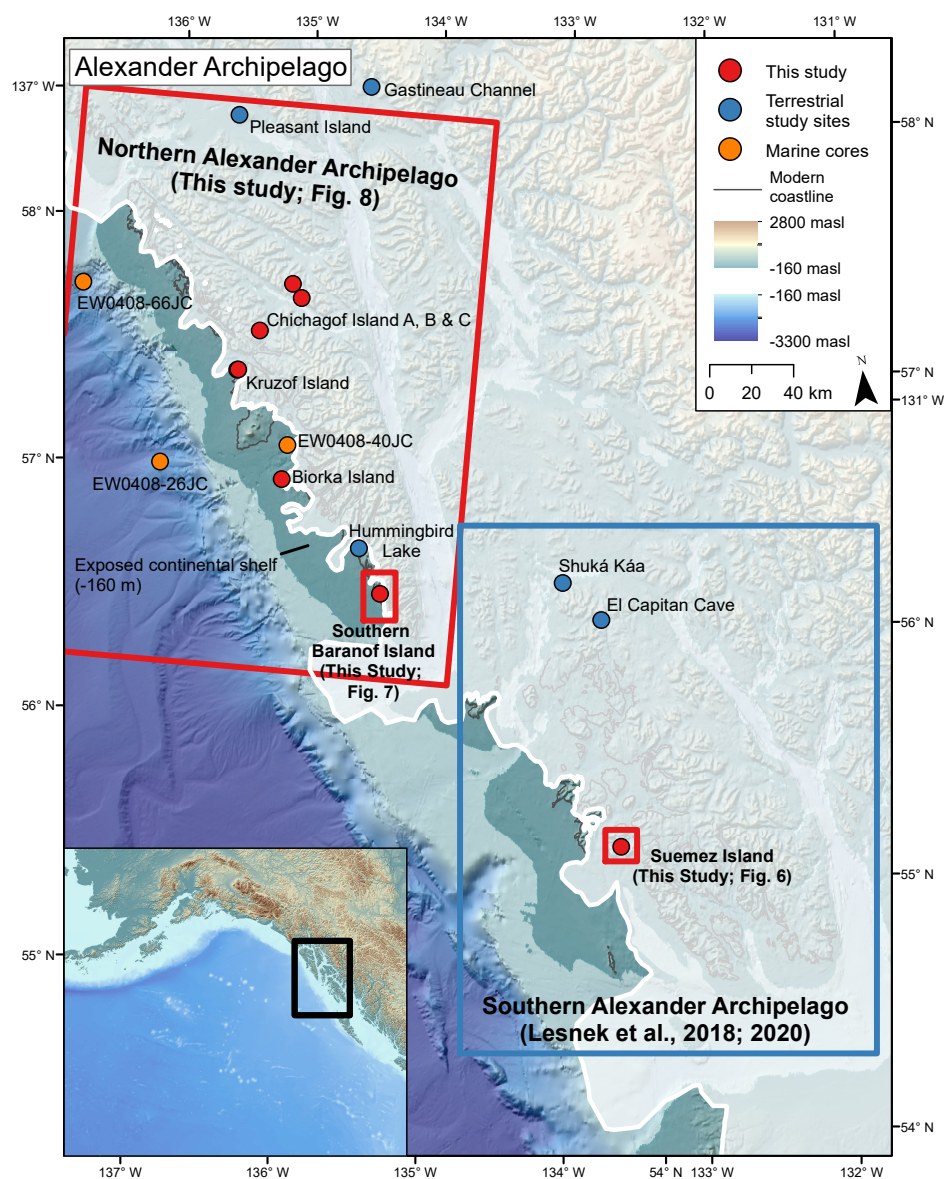
## 823 Figures and Tables



824

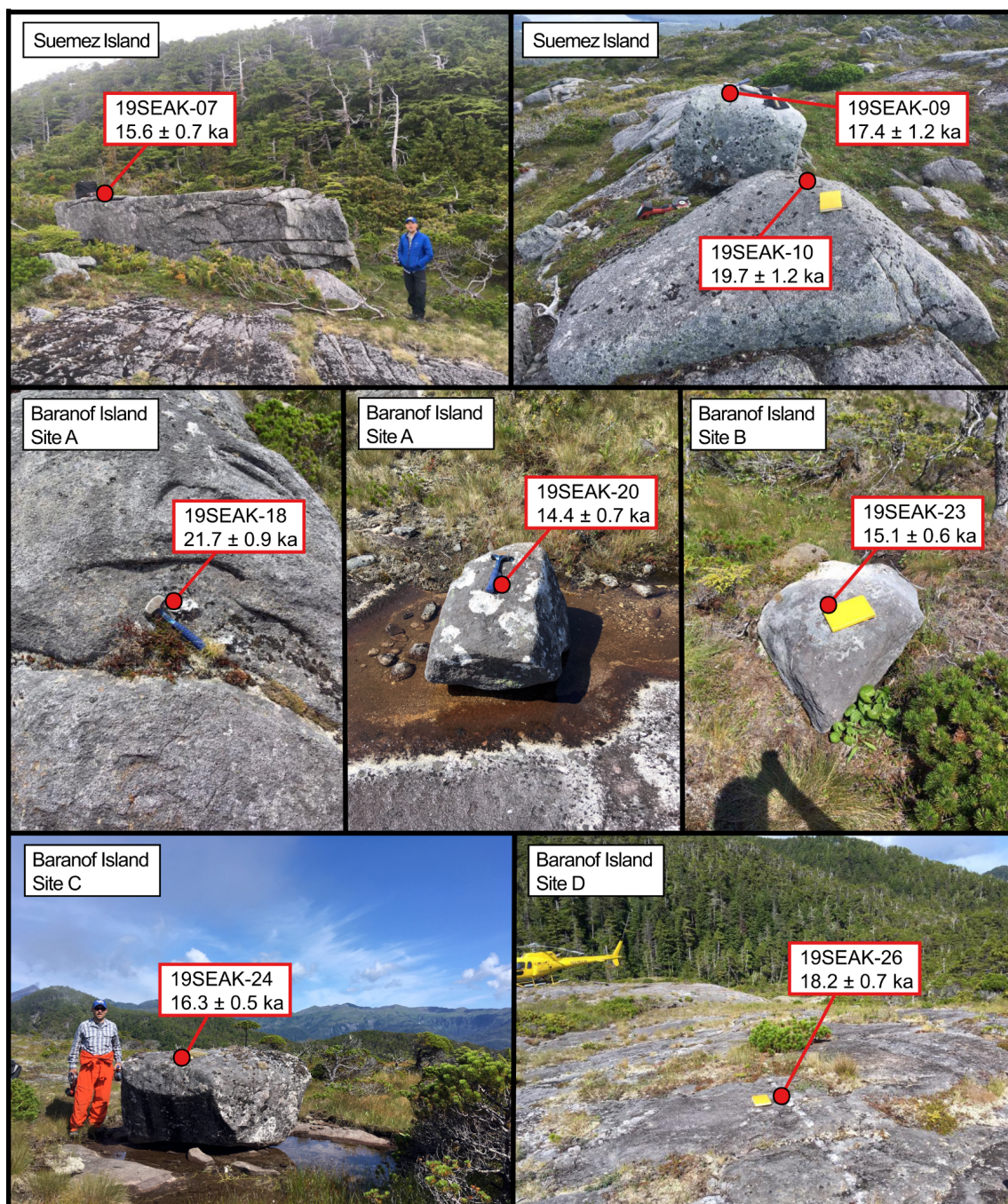
825 **Figure 1:** Map of the north Pacific region showing ice limits at 18.0 ka from Dalton et al. (2020)  
 826 with location of relevant sites mentioned in the text. The Alexander Archipelago is highlighted  
 827 by the red box on the main figure. Orange dots indicate locations of marine sediment cores: 51-  
 828 JPC (Caissie et al., 2010), SO202-27-6 (Maier et al., 2018), U1419 (Walczak et al., 2020),  
 829 EW0408-85JC (Davies et al., 2011; Praetorius and Mix, 2014; Praetorius et al., 2015), EW0408-  
 830 66JC (Praetorius and Mix, 2014; Praetorius et al., 2016), EW0408-26JC (Praetorius and Mix,  
 831 2014; Praetorius et al., 2016), EW0408-40JC (Addison et al., 2010), MD02-2496 (Cosma and  
 832 Hendy, 2008), and JT96-09 (Kienast and McKay, 2001). Blue dots indicate location of terrestrial  
 833 study sites: Sanak Island (Misarti et al., 2012), Kodiak Island (Mann and Peteet, 1994), Finger  
 834 Glacier (Mann 1986), Haida Gwaii (Clague et al., 1982; Mathewes and Clague, 1982), Calvert  
 835 Island, (Darvill et al., 2018), and Puget Sound (Porter and Swanson, 1998).





836  
837

838 **Figure 2:** The Alexander Archipelago showing relevant marine sediment cores and terrestrial  
 839 chronologies. Shaded white areas show hypothesized LLGM Cordilleran Ice Sheet extent  
 840 (Lesnek et al., 2020). - 160 m relative sea level lowering after Baichtal et al. (2021). Red boxes  
 841 and points show sampling locations from this study. Blue box shows extent of study area from  
 842 Lesnek et al. (2018; 2020). Orange dots represent locations of marine sediment cores: EW0408-  
 843 66JC and EW0408-26J (Praetorius and Mix, 2014; Praetorius et al., 2016) and EW0408-40JC  
 844 (Addison et al., 2010). Blue dots indicate locations of relevant terrestrial study sites: Gastineau  
 845 Channel (Miller, 1973), Pleasant Island (Hansen and Engstrom, 1996), Hummingbird Lake  
 846 (Ager, 2019), Shuká Káa (Lesnek et al., 2018), and El Capitan Cave (Wilcox et al., 2019).



847  
848

849 **Figure 3:** Sample photos from 2019 field season. All  $^{10}\text{Be}$  ages shown with  $1\sigma$  internal  
850 uncertainty.

851

852

853

854



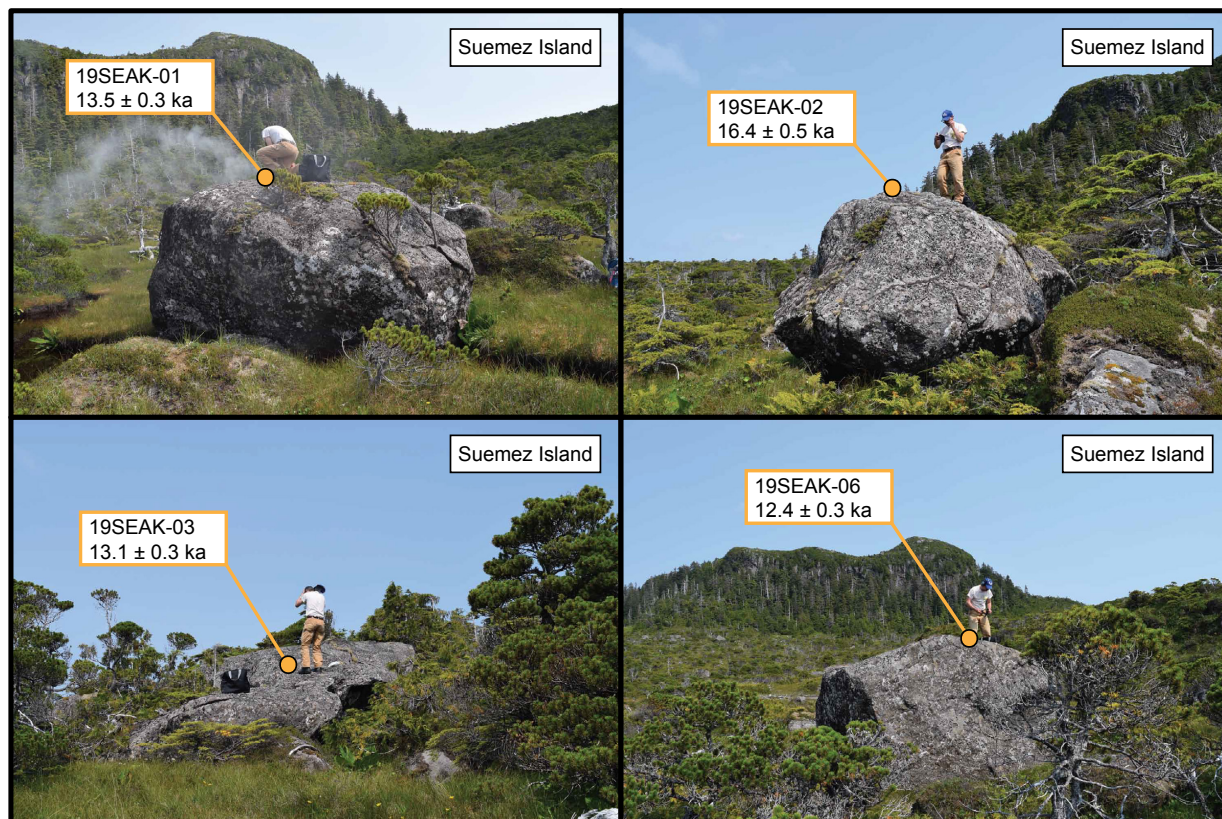
855

856

857 **Figure 4:** Sample photos from 2018 and 2020 field season. All  $^{10}\text{Be}$  ages are shown with  $1 \sigma$   
 858 internal uncertainty. Note the relatively small size of 20SEAK-15.

859

860



861  
862

863 **Figure 5:** Basalt samples and  $^{36}\text{Cl}$  ages from southwestern Suemez Island. Ages are reported at 1  
864  $\sigma$  internal uncertainty.

865  
866  
867  
868  
869  
870  
871  
872  
873  
874  
875  
876

Table 1:  $^{10}\text{Be}$  surface exposure age data

Sample ID	Sample type	Latitude ( $^{\circ}\text{N}$ ) <sup>a</sup>	Longitude ( $^{\circ}\text{W}$ ) <sup>a</sup>	Elevation (m asl) <sup>a</sup>	Boulder height (m)	Sample thickness (cm)	Topographic shielding correction	Quartz (g)	$^9\text{Be}$ added ( $\mu\text{g}$ )	$^{10}\text{Be}/^9\text{Be}$ ratio <sup>b</sup>	$^{10}\text{Be}/^9\text{Be}$ ratio uncertainty	$^{10}\text{Be}$ (atoms/g)	$^{10}\text{Be}$ uncertainty (atoms/g)	$^{10}\text{Be}$ age (ka) <sup>c</sup> Arctic PR	$^{10}\text{Be}$ age (ka) <sup>c</sup> Global PR
<b>BIORKA ISLAND</b>															
18JB005	Boulder	56.8482	-135.5314	47	1.0	3.0	1.0000	34.37	232	1.36E-13	4.38E-15	6.60E+04	2.12E+03	15.3 $\pm$ 0.5 (0.8)	14.7 $\pm$ 0.5 (1.2)
18JB006	Boulder	56.8471	-135.5315	43	1.2	3.0	1.0000	34.57	221	1.32E-13	4.87E-15	6.40E+04	2.35E+03	14.9 $\pm$ 0.6 (0.8)	14.3 $\pm$ 0.5 (1.2)
18JB007	Boulder	56.8527	-135.5363	46	1.0	3.0	1.0000	33.92	233	1.35E-13	4.54E-15	6.60E+04	2.23E+03	15.4 $\pm$ 0.5 (0.8)	14.8 $\pm$ 0.5 (1.1)
18JB008	Boulder	56.8528	-135.5362	46	1.0	3.0	1.0000	24.35	232	8.60E-14	2.92E-15	5.90E+04	1.99E+03	13.7 $\pm$ 0.5 (0.7)	13.2 $\pm$ 0.4 (1.1)
<b>SUEMEZ ISLAND</b>															
19SEAK-07	Boulder	55.2469	-133.3414	376	2.0	2.0	0.9958	21.24	233	1.25E-13	5.41E-15	9.19E+04	3.97E+03	15.6 $\pm$ 0.7 (0.9)	14.9 $\pm$ 0.6 (1.3)
19SEAK-08	Boulder	55.2470	-133.3419	392	1.0	2.0	0.9984	12.04	226	7.20E-14	5.42E-15	9.03E+04	6.80E+03	15.0 $\pm$ 1.1 (1.3)	14.4 $\pm$ 1.1 (1.5)
19SEAK-09	Boulder	55.2477	-133.3406	394	0.7	2.0	1.0000	19.44	233	1.31E-13	9.28E-15	1.05E+05	7.44E+03	17.4 $\pm$ 1.2 (1.4)	16.7 $\pm$ 1.2 (1.7)
19SEAK-10	Bedrock	55.2477	-133.3406	419	-	3.0	1.0000	17.81	213	1.38E-13	8.63E-15	1.21E+05	7.55E+03	19.7 $\pm$ 1.2 (1.4)	18.9 $\pm$ 1.2 (1.9)
<b>BARANOF ISLAND</b>															
<b>Site A</b>															
19SEAK-17	Boulder	55.3677	-134.9015	140	0.5	2.0	0.9923	25.08	233	1.30E-13	6.21E-15	8.02E+04	3.84E+03	16.9 $\pm$ 0.8 (1.0)	16.3 $\pm$ 0.8 (1.5)
19SEAK-18	Bedrock	56.3723	-134.9084	129	-	2.0	1.0000	25.24	232	1.66E-13	6.95E-15	1.02E+05	4.27E+03	21.7 $\pm$ 0.9 (1.2)	20.8 $\pm$ 0.9 (1.8)
19SEAK-19	Bedrock	56.3718	-134.9094	126	-	2.0	1.0000	24.80	233	2.10E-13	8.06E-15	1.31E+05	5.05E+03	28.0 $\pm$ 1.1 (1.5)	26.9 $\pm$ 1 (2.3)
19SEAK-20	Boulder	56.3712	-134.9082	135	0.6	2.0	1.0000	25.03	233	1.09E-13	5.59E-15	6.80E+04	3.47E+03	14.4 $\pm$ 0.7 (0.9)	13.8 $\pm$ 0.7 (1.3)
<b>Site B</b>															
19SEAK-21	Boulder	56.3636	-134.9068	48	0.5	2.0	1.0000	25.05	233	1.00E-13	4.57E-15	6.23E+04	2.84E+03	14.4 $\pm$ 0.7 (0.9)	13.8 $\pm$ 0.6 (1.2)
19SEAK-22	Bedrock	56.3636	-134.9072	58	-	2.0	0.9749	20.17	230	8.03E-14	3.10E-15	6.13E+04	2.36E+03	14.4 $\pm$ 0.6 (0.8)	13.8 $\pm$ 0.5 (1.2)
19SEAK-23	Boulder	56.3638	-134.9092	68	0.5	2.0	0.9911	20.24	231	8.64E-14	3.29E-15	6.60E+04	2.51E+03	15.1 $\pm$ 0.6 (0.8)	14.5 $\pm$ 0.6 (1.2)
<b>Site C</b>															
19SEAK-24	Boulder	56.3228	-134.892	150	1.0	1.5	1.0000	20.12	234	1.01E-13	3.39E-15	7.83E+04	2.63E+03	16.3 $\pm$ 0.5 (0.8)	15.6 $\pm$ 0.5 (1.3)
19SEAK-25	Bedrock	56.3231	-134.8916	163	-	1.5	1.0000	19.99	234	9.80E-14	3.41E-15	7.68E+04	2.67E+03	15.7 $\pm$ 0.6 (0.8)	15.1 $\pm$ 0.5 (1.3)
<b>Site D</b>															
19SEAK-26	Bedrock	56.3554	-134.8856	145	-	2	0.9879	25.12	235	1.37E-13	5.54E-15	8.56E+04	3.47E+03	18.2 $\pm$ 0.7 (1.0)	17.4 $\pm$ 0.7 (1.5)
19SEAK-27	Bedrock	56.3555	-134.8855	142	-	1.5	0.9963	25.04	233	1.54E-13	5.89E-15	9.59E+04	3.67E+03	20.2 $\pm$ 0.8 (1.1)	19.3 $\pm$ 0.7 (1.6)
<b>KRUZOF ISLAND</b>															
20SEAK-7	Boulder	57.3112	-135.8126	558	2.5	1.5	0.9976	20.14	233	1.36E-13	7.24E-15	1.05E+05	5.59E+03	14.9 $\pm$ 0.8 (1.0)	14.3 $\pm$ 0.8 (1.3)
20SEAK-10	Bedrock	57.3112	-135.8111	559	-	1.5	0.96912	20.13	231	1.20E-13	8.48E-15	9.23E+04	6.50E+03	13.4 $\pm$ 1.0 (1.1)	12.9 $\pm$ 0.9 (1.3)
20SEAK-12	Boulder	57.3110	-135.8110	569	1.0	1.0	0.9927	20.07	382	8.32E-14	3.74E-15	1.06E+05	4.77E+03	14.9 $\pm$ 0.7 (0.9)	14.3 $\pm$ 0.6 (1.3)
20SEAK-13	Boulder	57.3109	-135.8109	568.3	1.5	1.0	0.9941	20.25	230	1.36E-13	7.43E-15	1.04E+05	5.65E+03	14.6 $\pm$ 0.8 (1.0)	14.1 $\pm$ 0.8 (1.3)
<b>CHICHAGOF ISLAND</b>															
<b>Site A</b>															
20SEAK-14	Bedrock	57.4621	-135.6354	476	-	0.5	1.0000	20.25	230	1.34E-13	6.34E-15	1.01E+05	4.80E+03	15.3 $\pm$ 0.7 (0.9)	14.6 $\pm$ 0.7 (1.3)
20SEAK-15	Boulder	57.4621	-135.6354	476	0.3	1.0	1.0000	20.33	227	1.13E-13	6.04E-15	8.38E+04	4.50E+03	12.7 $\pm$ 0.7 (0.8)	12.2 $\pm$ 0.7 (1.1)
20SEAK-16	Boulder	57.4618	-135.6351	473	0.3	1.5	1.0000	20.26	240	7.48E-14	4.78E-15	5.92E+04	3.78E+03	9.0 $\pm$ 0.6 (0.7)	8.6 $\pm$ 0.6 (0.9)
<b>Site B</b>															
20SEAK-18	Boulder	57.5743	-135.2721	817	0.5	3.0	1.0000	15.20	226	1.09E-13	7.99E-15	1.09E+05	7.99E+03	12.4 $\pm$ 0.9 (1.0)	11.8 $\pm$ 0.9 (1.2)
20SEAK-19	Bedrock	57.5743	-135.2720	816	-	1.5	1.0000	20.05	239	1.57E-13	7.31E-15	1.25E+05	5.81E+03	14.1 $\pm$ 0.7 (0.8)	13.5 $\pm$ 0.6 (1.2)
<b>Site C</b>															
20SEAK-22	Bedrock	57.6425	-135.3483	779	-	2.0	1.0000	20.12	231	1.98E-13	8.58E-15	1.52E+05	6.59E+03	17.7 $\pm$ 0.8 (1.0)	17.0 $\pm$ 0.7 (1.5)

<sup>a</sup> Elevations and positions were recorded with a Garmin handheld GPS receiver (~5 m vertical uncertainty) or GAIA GPS (~5 m vertical uncertainty).

<sup>b</sup> AMS results from PRIME Lab are standardized to 07KNSTD (Nishiizumi et al., 2007); ratios are blank corrected and shown at 1 SD uncertainty.

<sup>c</sup>  $^{10}\text{Be}$  ages reported with one  $\sigma$  internal uncertainties; external uncertainties in parentheses; calculated with CRONUS-Earth calculator v. 3 (Balco et al., 2008) using the Arctic production rate (Young et al., 2013) or global production rate (Borchers et al., 2016) and Lm scaling.

**Table 2:**  $^{36}\text{Cl}$  surface exposure age data

Sample ID	Sample type	Latitude ( $^{\circ}\text{N}$ ) <sup>a</sup>	Longitude ( $^{\circ}\text{W}$ ) <sup>a</sup>	Elevation (m asl) <sup>a</sup>	Boulder height (m)	Sample thickness (cm)	Density ( $\text{g}/\text{cm}^3$ )	Topographic Shielding Correction	Aliquot dissolved for total Cl determination (g)	$^{37}\text{Cl}$ -enriched Cl added to total Cl aliquot ( $\mu\text{g}$ ) <sup>b</sup>	$^{35}\text{Cl}/^{37}\text{Cl}$ <sup>b</sup>	Total Cl concentration ( $\mu\text{g}/\text{g}$ )	Rock sample dissolved (g)	Natural Cl carrier added ( $\mu\text{g}$ ) <sup>c</sup>	$^{36}\text{Cl}/\text{Cl}$	$^{36}\text{Cl}/\text{Cl}$ Uncertainty <sup>d</sup>	$^{36}\text{Cl}$ concentration (atoms/g) <sup>e</sup>	$^{36}\text{Cl}$ concentration uncertainty (atoms/g) <sup>f</sup>	$^{36}\text{Cl}$ age (ka) <sup>f</sup>
<b>ROCK SAMPLES</b>																			
19SEAK-01 <sup>g</sup>	Boulder	55.2449	-133.4328	391	2.0	2.5	2.8	0.995658	1.2063	75.4	1.110	12.9 ± 0.8	12.0014	358	1.47E-13	3.39E-15	1.03E+05	2.41E+03	13.5 ± 0.3 (1.3)
19SEAK-02 <sup>h</sup>	Boulder	55.2461	-133.4327	398	2.5	3	2.8	0.994066	1.0383	76.2	1.014	5.7 ± 0.1	11.5081	435	1.74E-13	5.07E-15	1.27E+05	3.73E+03	16.4 ± 0.5 (1.5)
19SEAK-03 <sup>i</sup>	Boulder	55.246	-133.4324	398	2.0	2.5	2.8	0.994066	1.2061	76.5	1.282	24.0 ± 0.8	14.0301	171	2.00E-13	4.34E-15	1.22E+05	2.67E+03	13.1 ± 0.3 (1.3)
19SEAK-06 <sup>j</sup>	Boulder	55.2448	-133.4355	398	3.0	2	2.8	0.995524	1.2081	79.5	1.088	9.3 ± 0.6	20.0269	314	2.43E-13	5.09E-15	1.03E+05	2.16E+03	12.4 ± 0.3 (1.1)
<b>PROCESS BLANKS</b>																			
CLBLK-AQ4	-	-	-	-	-	-	-	-	-	78.0	0.953	-	-	-	-	-	-	-	-
CLBLK-AQ6	-	-	-	-	-	-	-	-	-	78.0	0.938	-	-	-	-	-	-	-	-
CLBLK-AQ8	-	-	-	-	-	-	-	-	-	76.6	0.936	-	-	-	-	-	-	-	-
CLBLK-26	-	-	-	-	-	-	-	-	-	-	-	-	-	0.1998	2.37E-15	9.24E-16	-	-	-

<sup>a</sup> Elevations and positions were recorded with a Garmin handheld GPS receiver (~5 m vertical uncertainty) or GAIA GPS (~5 m vertical uncertainty).

<sup>b</sup> The  $^{37}\text{Cl}$ -enriched spike was made at Lawrence Livermore National Laboratory. Its Cl concentration is 1285 ppm and its  $^{35}\text{Cl}/^{37}\text{Cl}$  ratio is 0.93.

<sup>c</sup> The natural Cl carrier was made by dissolving Weeks Island Halite in deionized water at the University of New Hampshire. Its Cl concentration is 1436 ± 9 ppm and its  $^{35}\text{Cl}/^{37}\text{Cl}$  ratio is 3.127.

<sup>d</sup> Uncertainties on  $^{35}\text{Cl}/^{37}\text{Cl}$  and  $^{36}\text{Cl}/\text{Cl}$  ratios and exposure ages represent propagated 1 $\sigma$  analytical uncertainties only

<sup>e</sup> Sample  $^{36}\text{Cl}$  concentrations are corrected for  $^{36}\text{Cl}$  contributed by process blank CLBLK-26

<sup>f</sup> Exposure ages are presented at 1 $\sigma$  internal uncertainty; external uncertainty shown in parentheses. Ages were calculated with the CRONUSEarth  $^{36}\text{Cl}$  calculator ([http://stoneage.ice-d.org/math/Cl36/v3/v3\\_Cl36\\_age\\_in.html](http://stoneage.ice-d.org/math/Cl36/v3/v3_Cl36_age_in.html)) and Lm scaling (Lal, 1991) assuming no surface erosion and steady state nucleogenic  $^{36}\text{Cl}$  production.

<sup>g</sup> Aliquot for stable Cl measurements processed with CLBLK-AQ6

<sup>h</sup> Aliquot for stable Cl measurements processed with CLBLK-AQ8

<sup>i</sup> Aliquot for stable Cl measurements processed with CLBLK-AQ4

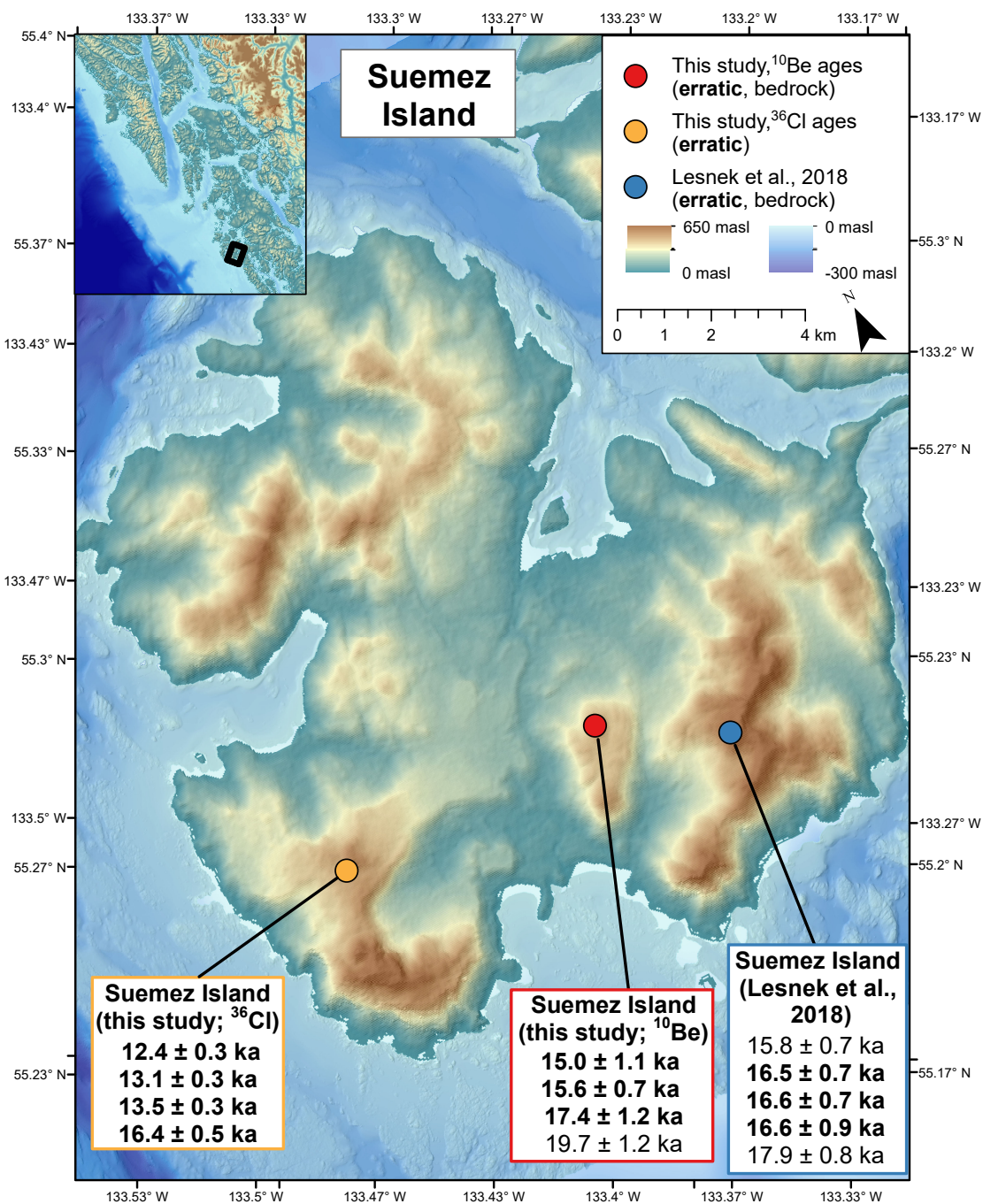


**Figure 6:**  $^{10}\text{Be}$  and  $^{36}\text{Cl}$  ages from samples collected on Suemez on island: red and yellow dots mark sampling site from this study, blue dot marks sampling site from Lesnek et al.(2018). Bold ages are from boulders; plain ages are from bedrock. All  $^{10}\text{Be}$  and  $^{36}\text{Cl}$  ages reported with  $1\sigma$  internal uncertainty.

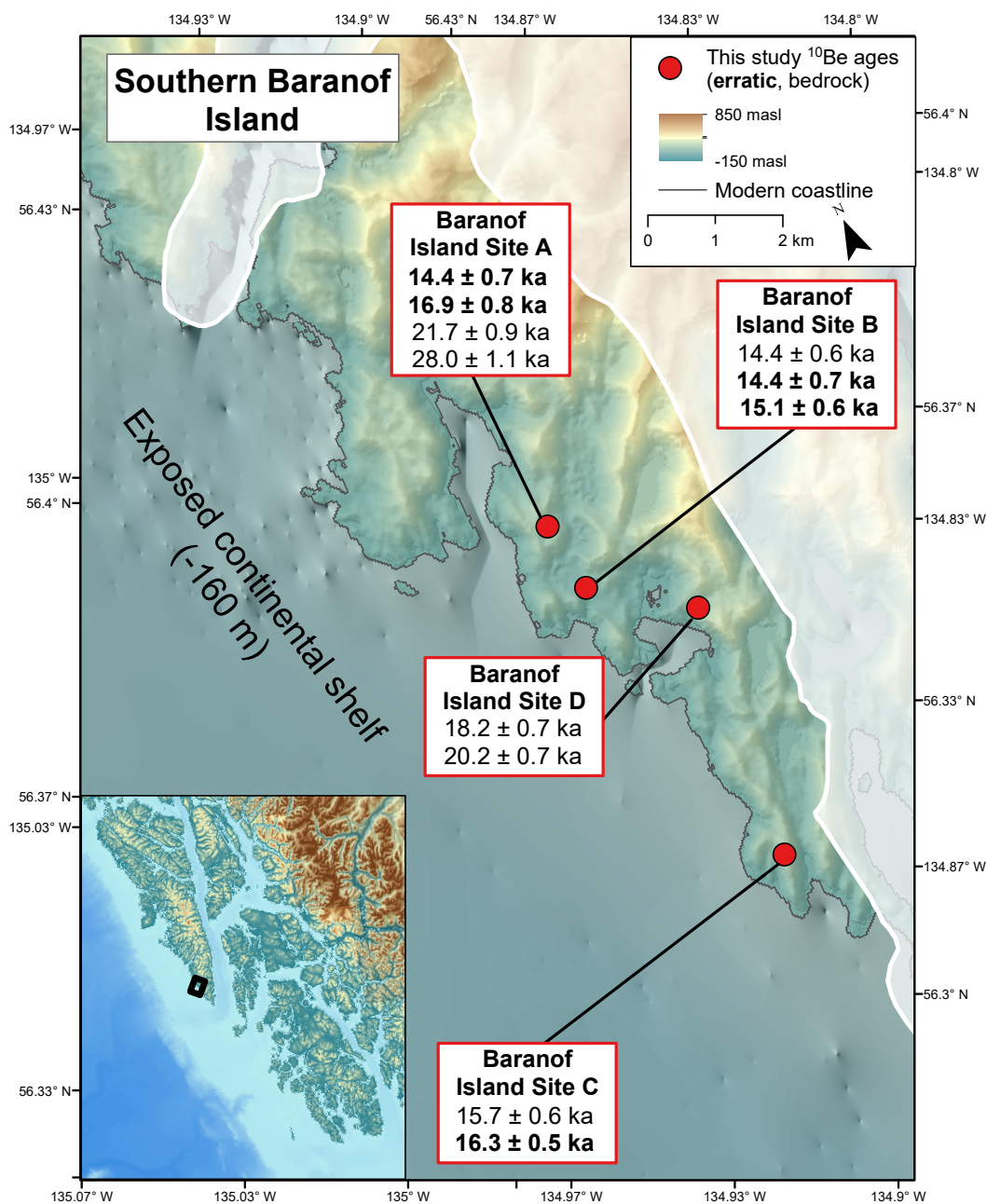


**Figure 7:**  $^{10}\text{Be}$  ages from sampling sites on southern Baranof Island. Bold ages are from boulders; plain ages are from bedrock. All ages are reported with  $1 \sigma$  internal error. Cordilleran Ice Sheet LGM extent after Carrara et al. (2007).



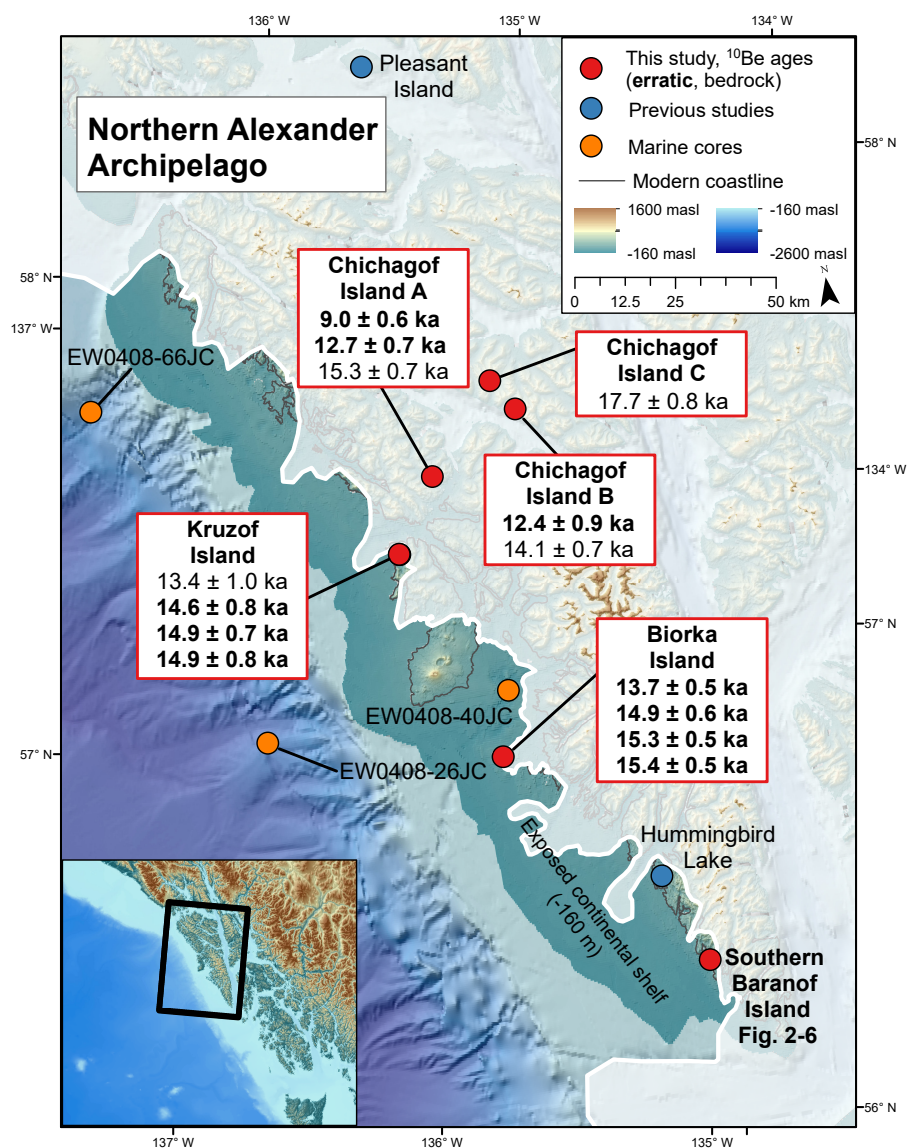


**Figure 8:**  $^{10}\text{Be}$  ages from sampling sites in the northern Alexander Archipelago. All ages are reported with  $1\sigma$  internal error. Bold ages are from boulders; plain ages are from bedrock.. LLGM Cordilleran Ice Sheet extent after Lesnek et al. (2020). Exposed continental shelf at -160 m below modern sea level Baichtal et al. (in press). Yellow dots show location of relevant marine sediment cores: EW0408-66JC and EW0408-26JC (Praetorius and Mix, 2014; Praetorius et al., 2016) and EW0408-40JC (Addison et al., 2010). Blue dots show locations of relevant terrestrial study sites: Pleasant Island (Hansen and Engstrom, 1996) and Hummingbird Lake (Ager, 2019).

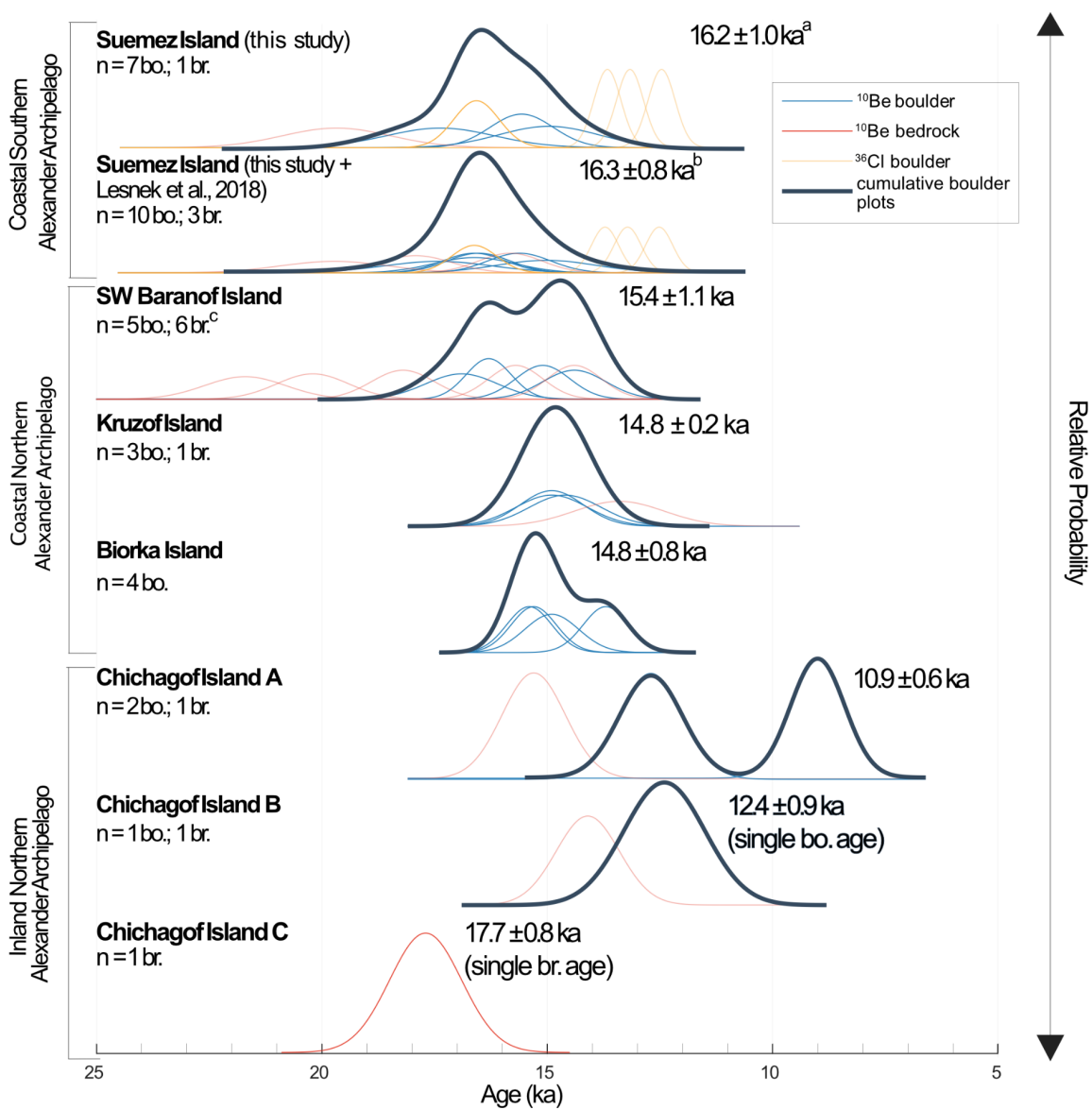


**Figure 9:** Relative probably plots of bedrock (red) and boulder (blue)  $^{10}\text{Be}$  and  $^{36}\text{Cl}$  boulder (yellow) ages from this study calculated with  $1\sigma$  internal uncertainty. bo. = boulder, br. = bedrock. All ages shown are mean ages from only boulders at each sample site reported with 1 SD unless noted. Cumulative plots represent all bold lines - transparent lines were not included in their calculation. <sup>a</sup>Average of all  $^{10}\text{Be}$  boulder ages and oldest  $^{36}\text{Cl}$  boulder age with 1 SD. <sup>b</sup>Average of all  $^{10}\text{Be}$  boulder ages (this study and Lesnek et al., 2018) and oldest  $^{36}\text{Cl}$  boulder age (this study). <sup>c</sup>One old outlier at  $28.0 \pm 1.1$  ka not shown.

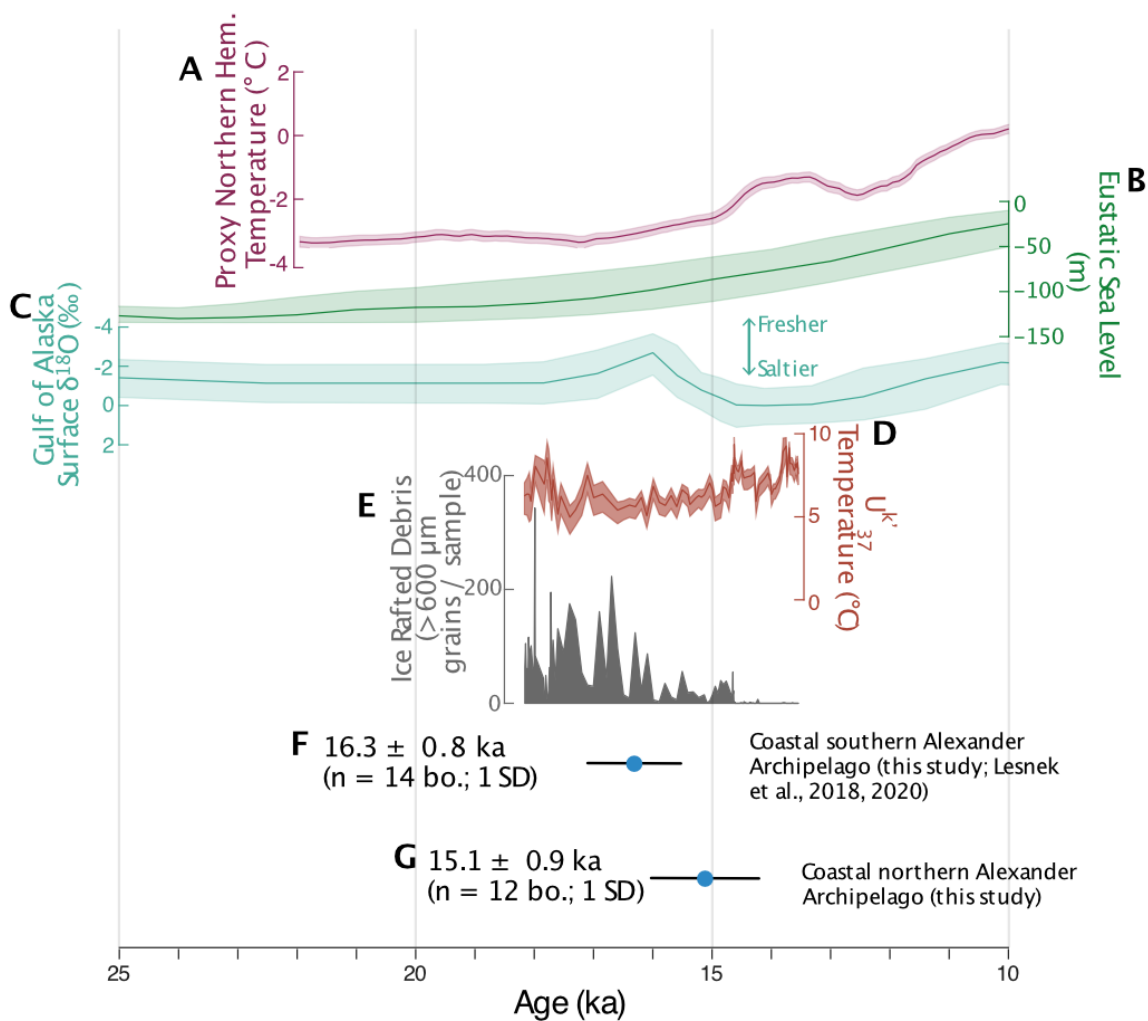


**Figure 10:** A) Proxy Northern Hemisphere temperature anomaly relative to early Holocene with  $1 \sigma$  error (Shakun et al., 2012). B) Eustatic sea-level curve (Spratt and Lisiecki, 2016). C) Gulf of Alaska surface salinity  $\delta^{18}O$  record (Core SO202-27-6; Maier et al., 2018). D) UK'37 temperature reconstruction from off the coast of the Alexander Archipelago (Cores EW0408-26JC, EW0408-66JC; Praetorius et al., 2016). E) Ice rafted debris record from off Vancouver Island (Core MD02-2496; Cosma et al., 2008). F) & G) Meanboulder  $^{10}\text{Be}$  ages from the coastal Alexander Archipelago, with  $1 \sigma$  r (this study; Lesnek et al., 2018; 2020).

